CD36 Drives Metastasis and Relapse in Acute Myeloid Leukemia

Thomas Farge, Jean Nakhle, Damien Lagarde, Guillaume Cognet, Nathaniel Polley, Rémy Castellano, Marie-Laure Nicolau, Claudie Bosc, Marie Sabatier, Ambrine Sahal, et al.

CD36 drives metastasis and relapse in acute myeloid leukemia

Thomas Farge[1,2,3,4,5,6†], Jean Nakhle[6†], Damien Lagarde[6,7,8], Guillaume Cognet[1,2,3], Nathaniel Polley[1,2,3], Rémy Castellano[9], Marie-Laure Nicolau[10,11], Claudie Bosc[1,2,3], Marie Sabatier[1,2,3], Ambrine Sahal[1,2,3], Estelle Saland[1,2,3], Yannick Jeanson[6], Nathan Guiraud[1,2,3], Emeline Boet[1,2,3], Camille Bergoglio[12], Mathilde Gotanègre[1,2,3], Pierre-Luc Mouchel[1,2,3,10,11], Lucille Stuani[1,2,3], Clément Larrue[1,2,3], Marie Sallese[6], Véronique De Mas[1,2,3,10,11], Cedric Moro[12], Cédric Dray[6], Yves Collette[9], Isabelle Raymond-Letron[6,13], Isabelle Ader[6], Christian Récher[1,2,3,10,11], Jean-Emmanuel Sarry[1,2,3], Florence Cabon[1,2,3‡], François Vergez[1,2,3,10,11‡], and Audrey Carrière[6‡*]

[1]Centre de Recherches en Cancérologie de Toulouse, Université de Toulouse, Inserm, CNRS, Toulouse, France.
[2]LabEx Toucan, Toulouse, France.
[3]Equipe Labellisée Ligue Nationale Contre le Cancer 2023, Toulouse, France.
[4]Institute of Metabolic and Cardiovascular Diseases, Team CERAMIC, INSERM, Paul Sabatier University, UMR1297, Toulouse, France
[5]Institut Fédératif de Biologie (IFB), CHU Toulouse, Toulouse, France
[6]RESTORE Research Center, Université de Toulouse, INSERM 1301, CNRS 5070, EFS, ENVT, Toulouse, France
[7]McGill University, Rosalind and Morris Goodman Cancer Institute, Montréal, Québec, Canada
[8]McGill University, Department of Biochemistry, Montréal, Québec, Canada
[9]Centre de Recherche en Cancérologie de Marseille, Aix-Marseille Univ, Inserm, CNRS, Institut Paoli-Calmettes, 13009 Marseille, France
[10]University of Toulouse, Toulouse, France.
[11]Centre Hospitalier Universitaire de Toulouse, Institut Universitaire du Cancer de Toulouse Oncopole, Service d'Hématologie, Université Toulouse III Paul Sabatier, Toulouse, France.
[12]Institute of Metabolic and Cardiovascular Diseases, Team MetaDiab, INSERM, Paul Sabatier University, UMR1297, Toulouse, France
[13]LabHPEC, Université de Toulouse, ENVT, Toulouse, France

[†] These authors contributed equally to this work

‡ These authors jointly supervised this work

* Corresponding author. Audrey Carrière, RESTORE Research Center, Bâtiment INCERE, 4bis avenue Hubert Curien, 31000 Toulouse, phone number: +33(0)534609513

audrey.carriere-pazat@inserm.fr

Short running title: CD36-dependent metastasis in acute myeloid leukemia

Conflict of interest statement: The authors declare no conflict of interest.

Keywords: acute myeloid leukemia, metastasis, CD36

SIGNIFICANCE

CD36 promotes blast migration and extramedullary disease in acute myeloid leukemia and represents a critical target that can be exploited for clinical prognosis and patient treatment.

ABSTRACT

Identifying mechanisms underlying relapse is a major clinical issue for effective cancer treatment. The emerging understanding of the importance of metastasis in hematological malignancies suggests that it could also play a role in drug resistance and relapse in acute myeloid leukemia (AML). In a cohort of 1,273 AML patients, we uncovered that the multifunctional scavenger receptor CD36 was positively associated with extramedullary dissemination of leukemic blasts, increased risk of relapse after intensive chemotherapy, and reduced event-free and overall survival. CD36 was dispensable for lipid uptake but fostered blast migration through its binding with thrombospondin-1. CD36-expressing blasts, which were largely enriched after chemotherapy, exhibited a senescent-like phenotype while maintaining their migratory ability. In xenograft mouse models, CD36 inhibition reduced metastasis of blasts and prolonged survival of chemotherapy-treated mice. These results pave the way for the development of CD36 as an independent marker of poor prognosis in AML patients and a promising actionable target to improve the outcome of patients.

INTRODUCTION

Acute myeloid leukemia (AML) is a heterogeneous group of diseases characterized by uncontrolled proliferation of clonal neoplastic hematopoietic precursor cells and impaired function of normal hematopoiesis, leading to neutropenia, anemia, and thrombocytopenia (1). If untreated, patients die of infection, bleeding, or organ failure, usually in a matter of weeks. Induction therapy, which combines 7 days of cytarabine (AraC) and 3 of anthracycline, is highly effective in killing leukemic cells, but despite a high rate of complete remission after these cytotoxic agents, most patients relapse (2). In AML patient-derived xenografts (PDX) in immunodeficient mice (non-obese diabetic scid gamma mouse, i.e. NSG) treated by AraC, we found CD36, a plasma membrane receptor and fatty acid transporter, among the most strongly upregulated genes in chemoresistant cells (3). In this study, we investigated the clinical relevance of this observation, and the mechanisms by which CD36 expression may contribute to chemoresistance and relapse.

We and others have shown that AML blasts are highly dependent on fatty acid metabolism and oxidative phosphorylation (OXPHOS) to bypass chemotherapy (3-5). In a number of tumors (6-8), an increased CD36 expression has been found to support cancer cell metabolism through the transport of fatty acids. However, CD36 is a multi-liganded receptor also binding molecules such as oxidized low-density lipoprotein (oxLDL) (9) or Thrombospondins 1 and 2 (TSP1 and TSP2) (10), and CD36 is involved in a number of functions besides metabolism, including angiogenesis, tumor immunity and metastasis (11-13). Metastatic cancers are largely resistant to treatments as compared to primary tumor cells, and represent the most frequent cause of death in cancer patients. In solid cancers as in leukemia (8,14), metastatic niches provide a microenvironment which fuels cell metabolism, protecting tumor cells from stresses and chemotherapies. Among the different mechanisms of relapse, entry of leukemic blasts into a senescent-like state is an important driver of chemoresistance and AML relapse (15). Senescent cells can stimulate tumor progression through their senescence-associated secretory phenotype (SASP) which comprises pro-inflammatory and pro-invasive molecules that can stimulate motility, invasion, and metastasis (16).

Until recently (17), because leukemic cells circulate in lymph and blood as their normal counterparts do, leukemia were generally not referred to as metastatic diseases. However, the presence at diagnosis of an extramedullary disease (EMD) in AML patients has been described for decades, with an incidence ranging from 2.5% (18) to 31% (19). The prognostic significance of EMD in AML was found as of no value in some studies (20), whereas others found EMD to convey a poor prognosis, independent of other established risk factors (18,19,21,22). These discrepancies between studies partly result from the difficulty to accurately score EMD. As recently shown in a multi-center cohort of AML patients, EMD was significantly associated with a decreased median overall survival (OS) and was predictive of a reduced even-free survival (EFS) only when histology was added to the clinical examination (22). This highlights the need to better understand the molecular mechanisms driving EMD and to identify reliable biomarkers. The impact of EMD in AML relapse after chemotherapy also needs to be deciphered.

Here, to uncover the molecular mechanisms behind dissemination of leukemic blasts in extramedullary organs, we combined *in vitro* and *in vivo* experiments using AML cell lines and patient cells, including single-cell analysis, alongside with a clinical study from a large cohort of 1,273 AML patients, some of whom have received an intensive chemotherapy regimen and have been followed for at least three years. Our findings highlight CD36 as an actionable driver of leukemic blasts metastasis and unravel new mechanisms contributing to AML relapse.

MATERIALS AND METHODS

Patients

Inclusion criteria were: newly diagnosed AML or relapse according to the WHO 2008 classification and age 15 years or older. This study included 1,273 patients admitted at the Hematology department of Toulouse University Hospital-IUCT-O and/or registered in the regional oncology network from January 1st 2016 to December 31st 2020 (TUH cohort). Data are gathered in an electronic clinical research form. A written informed consent was obtained from all patients in accordance with the Declaration of Helsinki, allowing the collection of clinical and biological data in an anonymized database. Samples from AML

patients were stored in the HIMIP collection (BB-0033-00060). In accordance with French law, the HIMIP collection was declared to the Ministry of Higher Education and Research (DC 2008-307 collection 1) and obtained a transfer agreement (AC 2008-129) after approval by the Comité de Protection des Personnes Sud-Ouest et Outremer II (ethics committee).

Cytogenetic and molecular risk classifications were in accordance with the Medical Research Council and ELN 2010 classifications, respectively (23,24). Details on treatment with first-line chemotherapy regimen used over time have been reported elsewhere (25). The decision-making process with regard to intensive or non-intensive treatment was based on initial characteristics such as white blood cell count, cytogenetics, age, secondary AML, performance status, and comorbidities. EMD status was determined at AML diagnosis by clinical examination.

Endpoints, including response, EFS, LFS, CIR and OS, were assessed according to standard criteria (1). Bone marrow assessment in patients treated with intensive chemotherapy was performed after blood recovery or in case of delayed recovery between day 35 and 45.

In vivo animal studies

NSG (NOD.Cg-Prkdcscid Il2rgtm1WjI/SzJ) mice were used for transplantation of AML cell lines or primary AML samples. Mice were housed in sterile conditions using HEPA-filtered micro-isolators and fed with irradiated food and sterile water in the Animal core facility of the Cancer Research Center of Toulouse (France). All animals were used in accordance with a protocol reviewed and approved by the Institutional Animal Care and Use Committee of Région Midi-Pyrénées (France). Six to 9 weeks-old male or female mice were randomly assigned to experimental groups before cell injection or drug treatments.

Primary patients sample phenotyping

Multi-parameter flow cytometry (MFC) was performed on whole bone marrow (BM) or blood specimens using a standard stain-lyse-wash procedure with ammonium chloride lysis. 1×10^5 cells were stained per analysis tube (see antibody list in **Table S1**), and data were acquired on at least 1×10^4 blasts when

specimen quality permitted. Data on standardized 8- to 10-color staining combinations were acquired on Navios instruments analyzed using Kaluza (Beckman-Coulter). A blasts gate including CD45 dim mononuclear cells was analyzed according to cytomorphologic data.

Xenograft mouse models

NSG mice were produced at the Genotoul Anexplo platform in Toulouse (France), using breeders obtained from Charles River Laboratories. To assess response to chemotherapy in PDX models, mice (6–9-week-old) were sublethally treated with busulfan (30 mg/kg) 24 h before injection of leukemic cells. Leukemia samples were thawed at 37 °C, washed in IMDM 20% FBS, and suspended in Hank's balanced salt solution at a final concentration of $2–10 \times 10^6$ cells in 200 µL for tail vein injection; 8–18 weeks after AML cell transplantation, once cell engraftment was confirmed by flow cytometry on peripheral blood or bone marrow aspirates, NSG mice were treated by daily intraperitoneal injection of 60 mg/kg AraC or vehicle (PBS) for 5 days. AraC was kindly provided by the pharmacy of the TUH. Mice were sacrificed at day 8 post-AraC treatment to harvest human leukemic cells from murine bone marrow.

To establish CLDX, NSG mice were treated with busulfan (20 mg/kg) 24 h before injection of AML cell lines. Cells were thawed and washed as previously described, suspended in HBSS at a final concentration of $0.2–2 \times 10^6$ in 200 µL before intravenous injection. Mice were treated by daily intraperitoneal injection of 30 mg/kg AraC for 5 days (starting day 10 for U937 and day 17 for OCIAML3 post-injection) and sacrificed at day 8 or later as indicated. When indicated, mice received concomitantly with AraC until sacrifice thrice weekly an intravenous injection of PBS (100 µL) containing either 5 µg of monoclonal CD36Ab FA6.152 (Stem Cell Technologies 60084) or 5 µg of mouse control IgG (Stem Cell Technologies 60070). Mice survival time was also determined. All animals were used in accordance with a protocol reviewed and approved by the Institutional Animal Care and Use Committee of Région Midi-Pyrénées (France).

^{14}C palmitate uptake and oxidation assay

Cells were preincubated for 3-hour with [1-^{14} C] palmitate (1 μCi/ml; Perkinelmer, Boston, MA) and non-labeled (cold) palmitate. Palmitate was coupled to a fatty acid-free BSA in a molar ratio of 5:1. Following incubation, ^{14}CO2 and ^{14}C-ASM were measured as previously described (26). Briefly, assayed medium is transferred into a custom-made Teflon 48-well trapping plate. The plate is clamped and sealed, and perchloric acid is injected through the perforations in the lid into the medium, which drives CO_2 through the tunnel into an adjacent well, where it is trapped in 1N NaOH. Following trapping, the media is spun twice and ^{14}C-ASM measured by scintillation counting. Aliquots of NaOH and medium are transferred into scintillation vials, and radioactivity is measured on a multipurpose scintillation counter (LS 6500; Beckman Coulter). All assays are performed in triplicates, and data are normalized to viable cell number.

RNA Extraction and Real-Time RT-qPCR.

Total cell RNA was isolated and extracted using the ZYMO RNA kit (Zymo). For mouse tissues, total RNA was isolated by Qiazol extraction and purified using RNeasy minicolumns (Qiagen, Hilden, Germany). 300-1000 ng total RNA was reverse transcribed using the High Capacity cDNA Reverse Transcription kit (Applied Biosystem 4368814), SYBR Green PCR Master Mix (Applied Biosystem 4309155), and 300 nmol/L primers on an Applied Biosystem (Massachusetts, United States) StepOne instrument. Relative gene expression was determined using the $2^{-\Delta CT}$ or $2^{-\Delta\Delta CT}$ method and normalized to m36B4 or hRPLP0 expression as described in Figure legends. Primer sequences are provided in Supplementary Material and methods.

Migration assay

For migration assays, 24 mm diameter, 8 μm pore transwells (Corning 353097) were used. Cell suspension in 0%FBS αMEM medium was added in the upper chamber. The lower chamber was filled with 500 μL of medium with or without 10% FBS. As indicated, anti-CD36 blocking antibodies (1

µg/mL) (FA6-152, Stem Cell Technologies 60084 or Cayman chemical JC63.1 10009893) and/or recombinant TSP1 (R&D Systems 3074-TH) were added in the upper chamber. Leukemic cells were allowed to migrate at 37°C for 24 hr. Inserts were removed and cell concentration was measured by cell counting with trypan blue coloration.

Immunohistochemistry

Subcutaneous adipose tissue samples were immediately immersed in 10% neutral buffered formalin fixative after sampling for 24 hours before storage in PBS at 4°C. After paraffin embedding, 3µm thickness paraffin sections were dewaxed (successive toluene and descending alcohols bathes) and stained with Haematoxilin and Eosin. Labeling of 3-µm sections of paraffin-embedded adipose tissues samples was performed out after antigen retrieval (Ptlink low pH, reference K8005, Dako) for 30 min, using anti-human specific Ku-80 antibody (2753S Cell Signaling, rabbit monoclonal antibody, dilution 1:150) and incubated for 50 min at room temperature. Staining was carried out with Dakostainer automated system using a biotinylated anti-rabbit antibody (reference ABK125 Microm) for 25 min at room temperature, followed by HRP (1:150, 25 min room temperature) and DAB as a chromogen. The stained slides were imaged by light microscopy on a Nikon Eclipse Ci-L microscope with a DS138 Fi3 Camera and NIS Elements D software.

Publicly accessible transcriptomic databases of AML patients used in this study

The following AML cohorts were used as indicated: GEO accession no. GSE14468 (Verhaak cohort (27)), BeatAML cohort (28), TCGA cohort (29). FAB M3 patients, and Patients who did not receive intensive chemotherapy were removed for analysis. Patients with overall survival value inferior to 1 year but still alive were removed in Kaplan-Meier curves. Other publicly accessible transcriptomic databases of AML patients used in this study were GSE40871, Klco et al. (30); GSE97631, Farge et al. (3); GSE146544, Duy et al. (15).

Establishment of the CD36 gene signature

Global analysis of frequency vs genes on normalized Affymetrix data showed that CD36 expression followed a Pareto distribution in TCGA and BEATAML databases whereas it followed a normal distribution in the Verhaak database. Only patients with non-zero CD36 expression were considered. In order to standardize the cutoff of differential expression among the three databases and establish experimental groups, based on a 95% confidence interval (i.e., p-value < 0.05) of CD36 expression, patients with a z-score > 1.64 were categorized as "High CD36" and < 1.64 as the baseline group. Welch's t-test of means for difference in variances was performed between the two groups to determine the differentially expressed genes. Then, data points were filtered to preserve overexpressed genes with a p-value < 0.05 in the High CD36 (positive "statistic") group. Corresponding test statistic values were then listed in decreasing order. Gene symbols were assigned unique Ensembl IDs to mitigate redundancies from gene synonyms and awkward formatting. The top 1000 genes in each database were used to select the common genes among the different databases.

Statistical analysis

For univariate survival analyses of OS and LFS in patients, Kaplan-Meier survival curves were drawn and differences in survival functions were tested using the Log-Rank test. Univariate survival analyses used Cumulative Incidence Functions and Gray's test for relapse (CIR), since non-relapse mortality was treated as competing events. Hazard Ratios (HR) and 95% confidence intervals (CI) were assessed using a standard Cox model, for OS and EFS and a proportional subdistribution hazard model which is an extension of the Cox model for the situation of competing risks, for CIR. All reported p-values were two-sided and the significance threshold was < 0.05. Statistical analyses were performed on STATA® version 13 (STATA Corp., College Station, TX).

We assessed the statistical analysis of the difference between two sets of data using two-tailed (non-directional) non-parametric Mann-Whitney test or unpaired test according to samples distribution, with or without Welch's correction depending on samples variance. For graphs with control condition normalized

to 1, we used a one sample t test with a hypothetical value set to 1. For multiple comparisons, one-way Anova or two-way Anova were performed with multiple comparison tests. For paired tests, Wilcoxon test was used. For contingency analysis of clinical data, we addressed Fisher's Exact test on raw data before normalization in percentages. For survival analyses, we used Log-rank (Mantel-Cox) test. Analyses were performed using Graphpad Prism (v9). A p value of less than 0.05 indicates significance. *$p < 0.05$; **$p < 0.01$; ***$p < 0.001$; ****$p < 0.0001$; ns, not significant.

Data Availability Statement

All raw data generated in this study are available upon request from the corresponding author. The data analyzed in this study were obtained from Gene Expression Omnibus (GEO) at GSE14468, GSE40871, GSE97631, GSE146544. Data from the BeatAML study was obtained from http://www.vizome.org, and TCGA AML dataset (29) was obtained from https://cbioportal.org.

RESULTS

CD36 is an independent prognostic marker of AML progression

To study if CD36 has a clinical prognostic value, we measured CD36 protein expression by flow cytometry in AML blasts of 1,273 AML patients from the Toulouse University Hospital (TUH). Based on the percentage of blasts expressing CD36 at diagnosis, AML patients were stratified as CD36-high (CD36-expressing blasts ≥ 20%, 407/1273, 32%) vs CD36-low (**Fig. 1a**). In this cohort, 435 AML patients were treated with an intensive chemotherapy regimen combining 3 days of daunorubicin or 5 days of idarubicin and 7 days of cytarabine. Although several features impact patients' prognosis, as already well described (1), a multivariate analysis revealed that CD36 was significantly associated with a worse event free survival (EFS; HR: 1.55; 95%CI: 1.17–2.05, p=0.002), and a worse overall survival (OS; HR: 1.69; 95%CI: 1.18–2.41, p=0.005; **Table 1**). Median EFS of CD36-high patients was half that of CD36-low patients (252 days vs 538 days respectively (HR:1.65, p<0.0001; **Fig. 1b**)), whereas median OS,

which was 462 days in CD36-high patients, was not reached after 3 years in CD36-low patients (HR: 1.88, p<0.0001; **Fig. 1c**). Furthermore, a high CD36 protein expression at diagnosis was associated with an increased cumulative incidence of relapse (CIR) after intensive chemotherapy (**Fig. 1d**), and a multivariate analysis showed that a high expression of CD36 was associated with a shorter CIR (SHR: 1.53; 95%CI: 1.07–2.19, p=0.02; **Table 1**). We next characterized the molecular and cytogenetic profile of patients exhibiting high percentage of CD36 expressing blasts. Consistent with our findings, intermediate and unfavorable karyotypes had higher percentage of CD36 expressing blasts (**Fig. 1e**). To provide an overview of the genomic landscape of CD36 AML clusters, we plotted targeted NGS data from 224 AML patients to examine the co-occurrence of mutations. We also calculated odds ratios for recurrent cytogenetic abnormalities. Comparison of the genomic landscape in 224 AML did not reveal a pattern related to CD36 expression, except for FLT3 abnormalities (**Fig. 1f-g**). We next examined the set of recurrent karyotype abnormalities (n=1202) showing an enrichment of AML with KMT2A (11q23) or t(9;22) abnormalities in CD36 high group and an increase in t(15;17) and t(8;21) AML in CD36 low group (**Fig. 1h**).

Altogether, these clinical findings obtained on a large patient cohort reveal that a high percentage of blasts expressing CD36 at diagnosis is an independent prognostic marker of disease progression, thus warranting the study of CD36 contribution to AML progression and relapse.

CD36 inhibition delays AML relapse after chemotherapy

Using additional PDX, we confirmed our previous observation (3) that AraC treatment *in vivo* induced a sustained increase in CD36 expression at the plasma membrane of residual AML blasts (**Fig. S1a-b**). To decipher whether CD36 is a promoter or a consequence of AML progression and relapse, we performed experiments using two human AML cell lines strongly expressing CD36 protein i.e. U937 and OCIAML3, U937 exhibiting two distinct subpopulations expressing low and high levels of CD36 at baseline, while OCIAML3 cells do not exhibit such phenotypical heterogeneity (**Fig. S1c)**. In both models, treating cells with AraC *in vitro* increased CD36 protein expression (**Fig. S1d**). Using shRNA, we knocked-down CD36

and then engrafted these cells and their control counterparts into NSG mice. After engraftment, mice were treated with vehicle or AraC for 5 days, and survival experiments were performed. In both models, knocking down CD36 did not affect the OS of untreated mice (data not shown) but significantly increased the survival of AraC-treated mice (**Fig. 2a-b)**. We then asked if CD36 inhibition might have a therapeutic potential once the disease was established. To this aim, we engrafted mice with U937 cells, and 10 days later randomized mice into four groups receiving vehicle only, AraC only, FA6-152 anti-CD36 blocking antibody only, or a combination of AraC and CD36 antibody. Whereas inhibition of CD36 did not increase the OS in untreated mice, AraC increased mice survival, and importantly, adding a CD36 antibody to AraC further significantly prolonged mice survival (**Fig. 2c**). Of note, neither CD36 knockdown with shRNA nor its inhibition with the FA6-152 blocking antibody affected the number of viable blasts **(Fig. S1e-h)**. Together, these data unveil a new therapeutic modality to potentialize chemotherapeutic effects, delaying time to relapse.

We then questioned the mechanisms behind CD36-dependent relapse after chemotherapy. We first hypothesized that CD36 mediates lipid transfer in leukemic blasts. Surprisingly, CD36 silencing by shRNA, which reduced CD36 protein expression in basal as well as in AraC-treated cells (**Fig. S1i-k)**, did not affect cell neutral lipid content, measured by Bodipy staining (**Fig. S1l-m**). Treatment with JC63.1 CD36 antibody which blocks fatty acid and oxLDL uptake (31,32) or with FA6-152 CD36 antibody which in addition inhibits CD36 binding to TSP1/2 (33-36) both failed to affect lipid content (**Fig. S1n-o**). Invalidation of CD36 using siRNA or FA6-152 CD36 blocking antibody did not affect ^{14}C-palmitate uptake and oxidation (**Fig. S1p-aa**), suggesting that CD36 is dispensable for lipid uptake in AML blasts.

To further investigate the role of CD36 in AML blast biology, we generated a CD36 gene signature comprising 249 genes that were all highly expressed along with CD36 in transcriptomic data from three AML patient databases (**Fig. 2d, Table S2**). Interestingly, this signature was enriched in primary AML cells treated with AraC compared to control cells in two different databases (GSE40871 (30), GSE146544 (15)), consistent with our previous observations (GSE97631) (3)) (**Fig. 2e**).

CD36 triggers blast migration

A Gene Ontology (GO) analysis of the above defined CD36 signature highlighted an enrichment in migration and adhesion processes (**Fig. 3a**), including the GO term "positive regulation of mononuclear cell migration" (**Fig. S2a**), while no enrichment for GO terms related to lipid transport and metabolism was found (data not shown). Considering that CD36 involvement in metastasis is described in several tumors (6,12,37), we hypothesized that CD36 could drive leukemic blast migration. Knocking-down CD36 with shRNA or siRNA decreased AML cell migration (**Fig. 3b and S2b-c**). FA6-152 CD36 blocking antibody, but not JC63.1 antibody, significantly decreased U937 and OCIAML3 migration (**Fig. 3c**; **Fig. S2d**). In fresh patient' samples, FA6-152 antibody decreased migration (**Fig. 3d**). FA6-152 antibody blocks the binding of CD36 to its ligand TSP1, which is well known to promote cell migration in various tumor models (38-40). Invalidation of TSP1 using shRNA (**Fig. S2e-f**) decreased migration of U937 (**Fig. 3e**) as well as of OCIAML3 cells (**Fig. S2g**). Adding A6.1 anti-TSP1 antibody also decreased U937 and OCIAML3 cell migration, and noteworthy, CD36 knock-down with shRNA abolished this effect **(Fig. 3f and S2h)**. Conversely, recombinant TSP1 increased migration of both U937 and OCIAML3 cells. This effect was hampered by the addition of CD36 blocking antibody (**Fig. 3g, Fig. S2i**), indicating that TSP1 promotes cell migration through its binding to CD36. As observed with FA6-152 anti-CD36 antibody, A6.1 TSP1 blocking antibody inhibited migration of fresh patient cells (**Fig. 3h**). Together, these data highlight that CD36 fosters AML blast migration, at least in part through its binding to TSP1.

Because migration is usually associated with metastasis in solid tumors, we asked whether blasts could migrate and localize into extramedullary organs. To visualize AML cell distribution *in vivo*, we injected a large panel of bioluminescent AML cell lines into NSG mice. In all models, AML cells localized throughout the body as shown by the acquisition of bioluminescence in mice during the time course of AML progression, and on isolated organs at sacrifice (**Fig.3i and Fig.S2j, k**). Analyses of human-specific CD45 expression by RT-qPCR in NSG mice grafted with U937 cells confirmed the presence of human blasts in the bone marrow, but also in different organs including spleen, perigonadal adipose tissues and

liver (**Fig. S2l**). Immunohistochemistry using a human-specific anti-Ku-80 antibody showed that AML blasts present in subcutaneous adipose tissues were scattered within the stroma, closely surrounding adipocytes **(Fig.3j)**, ruling out that the PCR results corresponded to blasts present in blood vessels. To further rule out that these extramedullary localizations might result from an experimental bias linked to the intravenous modality of blast injection, we injected OCIAML3 cells orthotopically into the right femur of NSG mice. Flow cytometry analyses revealed the presence of human CD45+ blasts in the contralateral femur, but also in spleen, subcutaneous adipose tissue, perigonadal adipose tissue and lung (**Fig. 3k**). This tissue distribution was comparable to that observed after intravenous injection of OCIAML3 cells (**Fig. S2m**), establishing that leukemic cells are able to migrate out of the bone marrow and engraft into distant locations. Interestingly, CD36 expression was increased in cells that had migrated from the site of injection, as shown comparing blasts from the bone marrow of injected femurs to contralateral femurs and extramedullary organs excepting lungs (**Fig. 3l**). In addition, we pretreated OCIAML3 cells with IGG or FA6-152 anti-CD36 antibody, injected these cells intra-venously into NSG mice which were then treated with either IGG or FA6-152 antibody. Ten days later, while untreated control cells started engrafting in the bone marrow (BM), perigonadal adipose tissue (PGAT), liver and lungs, minimal to no engraftment was detected in mice injected with FA6-152 pretreated cells **(Fig. S2n)**, suggesting that even in the absence of chemotherapy, CD36 is required for AML cell extravasation and migration. Altogether, these results establish that AML blasts can migrate from the bone marrow into different organs in xenograft models.

Residual blasts maintained their migratory properties after chemotherapy

We observed that treating cells with AraC increased CD11b, CD14, CD15 and CD44 protein expression levels (**Fig. 4a, Fig. S3a**), consistent with a AraC-induced partial differentiation of blasts towards a monocytic phenotype. Monocytes are particularly endowed with migratory capacities, and interestingly, a "Bone marrow monocyte" gene signature was enriched in primary AML cells treated with AraC as compared to control cells in three databases (GSE40871 (30), GSE97631 (3), GSE146544 (15)) (**Fig. 4b**).

We thus questioned the migration ability of blasts bypassing chemotherapy. Although to a lesser extent than in control conditions, U937 cells that survived 4 days of AraC treatment were still able to migrate, and, noteworthy, in both control and AraC-treated cells, CD36 blocking antibody FA6-152 decreased migration (**Fig. 4c**). We then studied the ability to migrate of viable CD36-high cells sorted after 4 days of treatment with AraC. While about 83% of U937 cells died, the percentage of living CD36-positive cells raised from 70% in untreated cells up to 90% in resistant ones and very few CD36-low cells survived, precluding their analysis (**Fig. 4d**). CD36 expression was strongly increased in migrating compared to non-migrating cells in both control and AraC-treated CD36-positive U937 cells (**Fig. 4e, f**). CD36-expressing blasts migrated more efficiently than CD36-negative cells in control condition, and, even though AraC partially decreased their migration, CD36-high cell were still efficiently migrating, similarly to untreated CD36-low cells (**Fig. 4g**).

We next engrafted mice with control or CD36 knocked-down U937 cells, treated mice with AraC for 5 days, and once disease relapse had translated into clinical signs, the presence of blasts was evaluated in different organs. At relapse, CD36 knock-down had increased the tumor burden in the bone marrow (**Fig. 4h**), while it had reduced it in the spleen (**Fig. 4i**) and in several extramedullary tissues (**Fig. 4j-m**), albeit not in the liver (data not shown). Thus, the increased time to relapse in mice co-treated with chemotherapy and CD36 inhibition (**Fig. 2a-c**) likely does not result from a blast reduction in the bone marrow but from a decreased blast dissemination into extramedullary organs.

Senescent-like state induced by cytarabine chemotherapy occurs specifically in CD36-high AML blasts

We observed that AraC treatment increased both cell size and granularity, two common features of senescent cells, and noteworthily, this increase almost exclusively occurred within the CD36-high viable cell population (**Fig. 5a-b**). In addition, senescence in AraC-treated cells translated into an increased β-galactosidase activity, which also occurred selectively in CD36-high cells, as measured by a 2.5-fold increase in C12FDG fluorescence (**Fig. 5c-d**). To confirm these data, we treated U937 cells for 4 days

with PBS or AraC, sorted viable CD36-high and -low cells and analyzed the expressions of several cyclin-dependent kinase inhibitors (*P21*, *P16*, *P15*), as well as that of cytokines of the SASP (*CCL2*, *IL1b*, *TNFa*). As previously (**Fig. 4d**), the very small number of CD36-low cells surviving after AraC treatment hindered these analyses. Expressions of all these well-established senescence markers were markedly increased by AraC treatment in CD36-high cells (**Fig. 5e**). Similarly, size, granularity, β-galactosidase activity and expressions of senescent markers, were all increased in chemoresistant OCIAML3 cells after 4 days of treatment with AraC (**Fig. S3b-d**), specifically in CD36-high cells (**Fig. S3b-c**). Interestingly, we found that *TSP1* mRNA, which was found to be part of the SASP (41), was strongly increased by AraC (**Fig. 5e, Fig.S3d)**, especially within the CD36-high population (**Fig. 5e)**. Of note, blocking CD36 with FA6-152 antibody did not alter AraC-induced increase in β-galactosidase activity of U937 or OCIAML3 cells (**Fig. 5f**, **Fig. S3e**). However, a significant decrease in SASP-related genes *TNFα* and *TSP1* mRNA level was observed in U937 cells, although no significant effect was observed regarding the expressions of other senescent markers (**Fig. 5g-m)**.

To decipher if senescence-like state and migration are functionally related, we compared the senescent profile of AraC-treated migrating and non-migrating cells. After 4 days of AraC or vehicle treatment, viable U937 cells were FACS-sorted and submitted to migration assay. In AraC-treated condition, β-galactosidase activity was increased in cells that had migrated compared to non-migrating cells (**Fig. S3f-g**), while no difference was found regarding expressions of CDKi and SASP related genes (data not shown). These data suggest that chemotherapy resistant cells that migrate preserve their senescent-like profile, and can even increase senescence-associated β-galactosidase activity. Together, these results show that chemotherapy increases the expressions of CD36 and its ligand TSP1 in blasts which retain their migration ability, and triggers a senescent-like phenotype specifically in CD36-high blasts, suggesting that senescent-like state and migration properties co-exist within CD36-high blasts bypassing chemotherapy.

Single-cell transcriptomic analysis reveals enrichment of CD36-high, migration and senescence-like gene signatures in a cluster emerging after standard chemotherapy

We next asked whether primary AML patients cells persisting after chemotherapy also exhibit a senescent-like state associated with migration *in vivo*. To this aim, we analyzed the transcriptomes of more than 30,000 single viable AML cells from a PDX model (TUH07 (42)) (**Fig. 6a**). The Seurat-based unsupervised hierarchical clustering analysis uncovered 8 distinct clusters before (PBS) and after AraC treatment (**Fig. 6b**). While the cell count within each cluster varied before and after AraC treatment, cluster 8 exhibited the highest increase in cell count after AraC treatment (**Table S3)**. A detailed analysis of cluster 8 revealed heterogeneity within this cluster, which consisted of two sub-clusters exhibiting either high or low expression of the CD36 gene signature (**Fig. 6c**). Strikingly, the sub-cluster highly expressing the CD36 gene signature was significantly enriched in gene sets related to both senescence and migration processes, with a large proportion of cells exhibiting a strong overlay between the two signatures (**Fig. 6c**). Correlation plots emphasized the global co-linearity among CD36, migration, and senescence across all cells, while the cluster 8 displayed the highest expression across all of the compared phenotypes (**Fig. S3h-j**). These findings further strengthened that migration and senescence-like states coexist within high CD36-expressing blasts enriched after chemotherapy *in vivo*.

CD36 is positively associated with extramedullary disease in AML patients

We assessed the clinical relevance of these findings in patients from the TUH cohort. Interestingly, patients with hyperleukocytosis had a higher percentage of CD36+ blasts (**Fig. 7a**). The presence of EMD at diagnosis was documented in 631 patients and among them, 166 (26.3%) exhibited EMD with 1, 2, or more than 2 organs involved, in agreement with other reports (19,20). In the TUH cohort, both EMD and a high CD36-positive blast percentage were independent prognostic factors of relapse and reduced OS (**Table S4**). We found that the presence of an EMD was significantly correlated with a higher percentage of CD36+ blasts at diagnosis (**Fig. 7b**), regardless of the number of organs involved (**Fig. 7c**). Analysis of CD36 expression in the bone marrow of patients from the TUH cohort showed a higher percentage of CD36 positive blasts in patients exhibiting minimal residual disease (MRD) after chemotherapy compared to patients without MRD (**Fig.7d**). Using a CD36-gating strategy in diagnosis/MRD paired patient

443 samples, we found a significant increase in cell size at MRD compared to diagnosis, a feature of senescent
444 cells, specifically in CD36-high patients (**Fig. 7e)**. Very interestingly, among patients classified as EMD-
445 negative, a high CD36 expression identified a group at higher risk for both CIR and reduced OS (**Fig. 7f-**
446 **g**). Together, these clinical data highlight that CD36 expression in blasts is positively associated with
447 EMD in patients.
448
449 **DISCUSSION**
450 Despite the availability in the recent years of new treatments targeting key survival and metabolic
451 vulnerabilities in leukemic blasts, AML remains an aggressive cancer with a poor prognosis, due to
452 frequent relapses after chemotherapy. Here, our study highlights CD36 as a prognostic marker and
453 therapeutic target of metastasis to thwart relapse in AML.
454 In patient- and -cell line-derived xenografts in NSG mice, we have previously found and here confirmed
455 that CD36 is overexpressed in chemoresistant blasts (3). While CD36 has been shown to support fatty acid
456 oxidation in chronic myeloid leukemia (8), our data suggest that, unlike FABP4 (43), CD36 is dispensable
457 for lipid metabolism in AML blasts. Although inhibiting lipid transport function of CD36 might require to
458 knock-out instead of knock-down its expression, as recently shown in AML (44), the absence of
459 significant enrichment in GO terms related to lipid metabolism in the CD36 gene signature constitutes an
460 additional evidence of the uncoupling between CD36 and lipid metabolism in leukemic blasts.
461 Strikingly, our work demonstrated that CD36 fosters AML blast migration. In xenografted mice, a wide
462 range of AML cell lines developed EMD in a variety of organs. This phenotype was also observed in the
463 immuno-competent syngeneic AML model MLL/AF9 (45), showing that EMD in NSG mice does not
464 result from an impaired immune response. Interestingly, AraC treatment, which increases CD36
465 expression, also triggers the differentiation of leukemic cells towards a monocytic phenotype. Monocytic
466 cells migrate out of the marrow to perform their functions in tissues. While chemotherapies were used in
467 lymphomas to enhance CD34+ hematopoietic stem cells mobilization in order to collect them before
468 autologous transplantation (46), their impact on leukemic blasts mobilization has not been investigated.

Importantly, while having no effect in untreated cells in contrast to findings obtained with MOLM13 cells (47), we demonstrated that CD36 inhibition delayed time to relapse after chemotherapy, as observed in a AML mouse model (44), this being associated with a decreased EMD.

Using a set of senescence markers, we demonstrated that chemotherapy-induced senescence occurs mostly, if not only, in CD36-high cells. While CD36 inhibition did not impair β-galactosidase activity, it decreased the expression of some senescence-related secreted factors including TNFα and TSP1. These results are in accordance with a recently published paper (48) showing that CD36 inhibition in muscle senescent cells, although not impacting β-galactosidase activity nor the number of senescent cells, decreased the expression of some SASP-related genes. This confers to CD36 a role in the secretory phenotype of senescent cells, as previously described (49). Together, these data suggest that CD36, rather than contributing to leukemic blasts entry into senescence, could play a role in the secretory phenotype of senescent blasts treated with chemotherapy AraC. Importantly, we demonstrated that AraC-surviving blasts were still able to migrate. The preservation of migratory abilities of CD36-high cells bypassing chemotherapy and exhibiting a senescence-like state was further strengthened by single-cell analysis of a PDX treated with AraC (42). A cell cluster emerging after chemotherapy was not only overexpressing the CD36 gene signature but also enriched in both senescence and migration gene sets. Among the components of the SASP that could support leukemic blasts migration, TSP1 was strongly increased by chemotherapeutic treatment, especially in the CD36-high cell population. The sustained induction of both CD36 and TSP1 by AraC treatment likely contributes to maintain the capacity of CD36-high cells to migrate, even after a chemotherapeutic stress.

The clinical relevance of these results was analyzed in a large cohort of 1,273 AML patients from the TUH. CD36 was found by multivariate analysis to be an independent marker of AML progression, with a higher hazard ratio than major parameters that are characteristic of aggressive AML (FLT3-ITD, adverse cytogenetics, etc.). A previous study performed on a smaller cohort (266 patients) also reported the poor outcome of AML patients with a high CD36 expression (50). In the TUH cohort, the pejorative role of CD36 is further emphasized by the fact that patients with MRD after induction chemotherapy had a higher

percentage of CD36-positive blasts at diagnosis than patients without MRD. Interestingly, both leukocytosis and EMD were significantly associated with a high percentage of CD36-positive blasts at diagnosis and EMD was found to convey a poor prognosis, as recently shown (22). Importantly, among patients classified as EMD-negative, CD36 expression, whose evaluation is easily performed in routine practice, discriminated a group of patients with a higher CIR and a reduced OS. The impact of CD36 on patients classification is reinforced by the fact that its expression is not clearly associated with mutational profiles commonly utilized in clinical practice for AML.

The present study has some limitations. Inhibition of CD36 by shRNA or blocking antibodies did not impact lipid uptake in leukemic blasts. These methods however do not result in complete loss of CD36 activity and it is thus possible that the amount of protein remaining active is sufficient to allow normal lipid metabolism in blasts. CD36 knockout by genetic approaches, although not clinically easy to duplicate, could reveal a role of CD36 in lipid metabolism in leukemic blasts. We showed that CD36 fosters leukemic blasts migration, at least in part through its binding with TSP1 which was strongly released by blasts surviving chemotherapy. However, one cannot rule out the possibility that TSP1 may also be secreted by the microenvironment of different organs in response to chemotherapy which could impact blasts metastasis.

In conclusion, whereas most AML studies are focused on leukemic cells present in the bone marrow, our study unravels the importance of blast dissemination and EMD triggered by AraC. It highlights the non-canonical role of CD36 in this process, opening a new therapeutic strategy through CD36 inhibition in combination to chemotherapy to impair this metastatic process.

ACKNOWLEDGEMENTS

We thank all members of mice core facilities (UMS006, ANEXPLO, Inserm, Toulouse) in particular Marie Lulka, Christine Campi, Sarah Gandarillas and Cédric Baudelin for their support and technical

assistance, and Eric Delabesse for the management of the Biobank BRC-HIMIP that is supported by CAPTOR. This work was granted access to the HPC resources of CALMIP supercomputing center under the allocation 2019-T19001. Team JE Sarry is a member of OPALE Carnot Institute, The Organization for Partnerships in Leukemia. We thank Anne-Marie Benot, Muriel Serthelon and Stéphanie Nevouet for their daily help about the administrative and financial management of our team. We are grateful to the CERT platform from RESTORE, in particular Marie-Laure Renoud and Jessica Fontaine, for flow cytometry facilities as well as Sophie Bonnel, Lucas Bourdens, Claire Maslo, and Anais Checkroun for their help in experiments. We thank Mrs Zakaroff-Girard and Riant (Cytometry Core Facility, Inserm U1048, part of TRI Imaging Platform, Genotoul) and Mrs Farce (The Technology Cluster's Cytometry and Cell Sorting Platform, CRCT) for cell-sorting technical assistance. We thank Catherine Muller and Camille Attané from the Institut de Pharmacologie et de Biologie Structurale (IPBS), Beatrice Cousin, Vincent Cuminetti and Louis Casteilla from STROMALab/RESTORE for very helpful discussions and Armelle Yart from RESTORE for manuscript reviewing.

GRANT SUPPORT

This work was also supported by the Programme "Investissement d'Avenir" PSPC (IMODI; JE Sarry), the Laboratoire d'Excellence Toulouse Cancer (TOUCAN and TOUCAN2.0; contract ANR11-LABEX; JE Sarry), INCA (PLBIO 2020-010, DIALAML; JE Sarry), the Fondation Toulouse Cancer Santé (BADIPAML; JE Sarry), the Fondation ARC, the Cancéropôle Grand Sud-Ouest, the Ligue Nationale de Lutte Contre le Cancer, the association Prolific and the association GAEL. A.S. is a fellow from the European Regional Development Fund through the Interreg V-A Spain-France-Andorra (POCTEFA) program, project PROTEOblood (EFA360/19; JE Sarry). T.F. has a fellowship from the Fondation Toulouse Cancer Santé and Fondation ARC. This work was supported by the National Research Agency (ANR: Agence Nationale de la Recherche) for the "Investissement d'avenir" (ANR-11-PHUC-001, CAPTOR research program; JE Sarry) and in part by ANR-21-CE14-0057-01 (C.M.).

AUTHOR CONTRIBUTIONS

Conceptualization: TF, JN, IA, JES, CR, FV, FC, AC

Methodology: TF, JN, RC, YC, CM, IA, JES, FV, FC, AC

Investigation: TF, JN, DL, GC, NP, RC, MLN, CB, MSab, AS, ES, YJ, NG, EB, CB, MG, PLM, LS, CL, MSal, VDM, IRL

Funding acquisition: FV, CR, IA, JES, FC, AC

Supervision: FV, FC, AC

Writing – original draft: TF, FV, FC, AC

Writing – review & editing: TF, JN, DL, GC, NP, RC, LS, CM, CD, YC, IRL, IA, CR, JES, FV, FC, AC

COMPETING INTERESTS STATEMENT

The authors declare no conflict of interest.

SUPPLEMENTARY MATERIALS

REFERENCES

1. Dohner H, Estey E, Grimwade D, Amadori S, Appelbaum FR, Buchner T*, et al.* Diagnosis and management of AML in adults: 2017 ELN recommendations from an international expert panel. Blood **2017**;129:424-47
2. Short NJ, Konopleva M, Kadia TM, Borthakur G, Ravandi F, DiNardo CD*, et al.* Advances in the Treatment of Acute Myeloid Leukemia: New Drugs and New Challenges. Cancer Discov **2020**;10:506-25
3. Farge T, Saland E, de Toni F, Aroua N, Hosseini M, Perry R*, et al.* Chemotherapy-Resistant Human Acute Myeloid Leukemia Cells Are Not Enriched for Leukemic Stem Cells but Require Oxidative Metabolism. Cancer Discov **2017**;7:716-35
4. Boyd AL, Aslostovar L, Reid J, Ye W, Tanasijevic B, Porras DP*, et al.* Identification of Chemotherapy-Induced Leukemic-Regenerating Cells Reveals a Transient Vulnerability of Human AML Recurrence. Cancer Cell **2018**;34:483-98 e5
5. van Gastel N, Spinelli JB, Sharda A, Schajnovitz A, Baryawno N, Rhee C*, et al.* Induction of a Timed Metabolic Collapse to Overcome Cancer Chemoresistance. Cell Metab **2020**;32:391-403 e6
6. Ladanyi A, Mukherjee A, Kenny HA, Johnson A, Mitra AK, Sundaresan S*, et al.* Adipocyte-induced CD36 expression drives ovarian cancer progression and metastasis. Oncogene **2018**;37:2285-301
7. Feng WW, Wilkins O, Bang S, Ung M, Li J, An J*, et al.* CD36-Mediated Metabolic Rewiring of Breast Cancer Cells Promotes Resistance to HER2-Targeted Therapies. Cell Rep **2019**;29:3405-20 e5
8. Ye H, Adane B, Khan N, Sullivan T, Minhajuddin M, Gasparetto M*, et al.* Leukemic Stem Cells Evade Chemotherapy by Metabolic Adaptation to an Adipose Tissue Niche. Cell Stem Cell **2016**;19:23-37
9. Endemann G, Stanton LW, Madden KS, Bryant CM, White RT, Protter AA. CD36 is a receptor for oxidized low density lipoprotein. J Biol Chem **1993**;268:11811-6
10. Asch AS, Barnwell J, Silverstein RL, Nachman RL. Isolation of the thrombospondin membrane receptor. J Clin Invest **1987**;79:1054-61
11. Deng M, Cai X, Long L, Xie L, Ma H, Zhou Y*, et al.* CD36 promotes the epithelial-mesenchymal transition and metastasis in cervical cancer by interacting with TGF-beta. J Transl Med **2019**;17:352
12. Pascual G, Avgustinova A, Mejetta S, Martin M, Castellanos A, Attolini CS*, et al.* Targeting metastasis-initiating cells through the fatty acid receptor CD36. Nature **2017**;541:41-5
13. Silverstein RL, Febbraio M. CD36, a scavenger receptor involved in immunity, metabolism, angiogenesis, and behavior. Sci Signal **2009**;2:re3
14. Ye H, Minhajuddin M, Krug A, Pei S, Chou CH, Culp-Hill R*, et al.* The Hepatic Microenvironment Uniquely Protects Leukemia Cells through Induction of Growth and Survival Pathways Mediated by LIPG. Cancer Discov **2021**;11:500-19
15. Duy C, Li M, Teater M, Meydan C, Garrett-Bakelman FE, Lee TC*, et al.* Chemotherapy Induces Senescence-Like Resilient Cells Capable of Initiating AML Recurrence. Cancer Discov **2021**;11:1542-61
16. Kyjacova L, Saup R, Ronsch K, Wallbaum S, Dukowic-Schulze S, Foss A*, et al.* IER2-induced senescence drives melanoma invasion through osteopontin. Oncogene **2021**;40:6494-512
17. Whiteley AE, Price TT, Cantelli G, Sipkins DA. Leukaemia: a model metastatic disease. Nat Rev Cancer **2021**;21:461-75
18. Chang H, Brandwein J, Yi QL, Chun K, Patterson B, Brien B. Extramedullary infiltrates of AML are associated with CD56 expression, 11q23 abnormalities and inferior clinical outcome. Leuk Res **2004**;28:1007-11

19. Cribe AS, Steenhof M, Marcher CW, Petersen H, Frederiksen H, Friis LS. Extramedullary disease in patients with acute myeloid leukemia assessed by 18F-FDG PET. Eur J Haematol **2013**;90:273-8
20. Ganzel C, Manola J, Douer D, Rowe JM, Fernandez HF, Paietta EM*, et al.* Extramedullary Disease in Adult Acute Myeloid Leukemia Is Common but Lacks Independent Significance: Analysis of Patients in ECOG-ACRIN Cancer Research Group Trials, 1980-2008. J Clin Oncol **2016**;34:3544-53
21. Byrd JC, Weiss RB, Arthur DC, Lawrence D, Baer MR, Davey F*, et al.* Extramedullary leukemia adversely affects hematologic complete remission rate and overall survival in patients with t(8;21)(q22;q22): results from Cancer and Leukemia Group B 8461. J Clin Oncol **1997**;15:466-75
22. Eckardt JN, Stolzel F, Kunadt D, Rollig C, Stasik S, Wagenfuhr L*, et al.* Molecular profiling and clinical implications of patients with acute myeloid leukemia and extramedullary manifestations. J Hematol Oncol **2022**;15:60
23. Grimwade D, Hills RK, Moorman AV, Walker H, Chatters S, Goldstone AH*, et al.* Refinement of cytogenetic classification in acute myeloid leukemia: determination of prognostic significance of rare recurring chromosomal abnormalities among 5876 younger adult patients treated in the United Kingdom Medical Research Council trials. Blood **2010**;116:354-65
24. Dohner H, Estey EH, Amadori S, Appelbaum FR, Buchner T, Burnett AK*, et al.* Diagnosis and management of acute myeloid leukemia in adults: recommendations from an international expert panel, on behalf of the European LeukemiaNet. Blood **2010**;115:453-74
25. Bertoli S, Tavitian S, Huynh A, Borel C, Guenounou S, Luquet I*, et al.* Improved outcome for AML patients over the years 2000-2014. Blood Cancer J **2017**;7:635
26. Laurens C, Bourlier V, Mairal A, Louche K, Badin PM, Mouisel E*, et al.* Perilipin 5 fine-tunes lipid oxidation to metabolic demand and protects against lipotoxicity in skeletal muscle. Sci Rep **2016**;6:38310
27. Verhaak RG, Wouters BJ, Erpelinck CA, Abbas S, Beverloo HB, Lugthart S*, et al.* Prediction of molecular subtypes in acute myeloid leukemia based on gene expression profiling. Haematologica **2009**;94:131-4
28. Tyner JW, Tognon CE, Bottomly D, Wilmot B, Kurtz SE, Savage SL*, et al.* Functional genomic landscape of acute myeloid leukaemia. Nature **2018**;562:526-31
29. Cancer Genome Atlas Research N, Ley TJ, Miller C, Ding L, Raphael BJ, Mungall AJ*, et al.* Genomic and epigenomic landscapes of adult de novo acute myeloid leukemia. N Engl J Med **2013**;368:2059-74
30. Klco JM, Spencer DH, Lamprecht TL, Sarkaria SM, Wylie T, Magrini V*, et al.* Genomic impact of transient low-dose decitabine treatment on primary AML cells. Blood **2013**;121:1633-43
31. Mwaikambo BR, Sennlaub F, Ong H, Chemtob S, Hardy P. Activation of CD36 inhibits and induces regression of inflammatory corneal neovascularization. Invest Ophthalmol Vis Sci **2006**;47:4356-64
32. Klenotic PA, Page RC, Li W, Amick J, Misra S, Silverstein RL. Molecular basis of antiangiogenic thrombospondin-1 type 1 repeat domain interactions with CD36. Arterioscler Thromb Vasc Biol **2013**;33:1655-62
33. Corbet C, Bastien E, Santiago de Jesus JP, Dierge E, Martherus R, Vander Linden C*, et al.* TGFbeta2-induced formation of lipid droplets supports acidosis-driven EMT and the metastatic spreading of cancer cells. Nat Commun **2020**;11:454
34. Nergiz-Unal R, Lamers MM, Van Kruchten R, Luiken JJ, Cosemans JM, Glatz JF*, et al.* Signaling role of CD36 in platelet activation and thrombus formation on immobilized thrombospondin or oxidized low-density lipoprotein. J Thromb Haemost **2011**;9:1835-46
35. Ohgami N, Nagai R, Ikemoto M, Arai H, Kuniyasu A, Horiuchi S*, et al.* CD36, a member of class B scavenger receptor family, is a receptor for advanced glycation end products. Ann N Y Acad Sci **2001**;947:350-5

36. Aburima A, Berger M, Spurgeon BEJ, Webb BA, Wraith KS, Febbraio M*, et al.* Thrombospondin-1 promotes hemostasis through modulation of cAMP signaling in blood platelets. Blood **2021**;137:678-89
37. Gong J, Lin Y, Zhang H, Liu C, Cheng Z, Yang X*, et al.* Reprogramming of lipid metabolism in cancer-associated fibroblasts potentiates migration of colorectal cancer cells. Cell Death Dis **2020**;11:267
38. Sargiannidou I, Qiu C, Tuszynski GP. Mechanisms of thrombospondin-1-mediated metastasis and angiogenesis. Semin Thromb Hemost **2004**;30:127-36
39. Firlej V, Mathieu JR, Gilbert C, Lemonnier L, Nakhle J, Gallou-Kabani C*, et al.* Thrombospondin-1 triggers cell migration and development of advanced prostate tumors. Cancer Res **2011**;71:7649-58
40. Hu C, Wen J, Gong L, Chen X, Wang J, Hu F*, et al.* Thrombospondin-1 promotes cell migration, invasion and lung metastasis of osteosarcoma through FAK dependent pathway. Oncotarget **2017**;8:75881-92
41. Mikula-Pietrasik J, Sosinska P, Janus J, Rubis B, Brewinska-Olchowik M, Piwocka K*, et al.* Bystander senescence in human peritoneal mesothelium and fibroblasts is related to thrombospondin-1-dependent activation of transforming growth factor-beta1. Int J Biochem Cell Biol **2013**;45:2087-96
42. Bosc C, Saland E, Bousard A, Gadaud N, Sabatier M, Cognet G*, et al.* Mitochondrial inhibitors circumvent adaptive resistance to venetoclax and cytarabine combination therapy in acute myeloid leukemia. Nat Cancer **2021**;2:1204-23
43. Shafat MS, Oellerich T, Mohr S, Robinson SD, Edwards DR, Marlein CR*, et al.* Leukemic blasts program bone marrow adipocytes to generate a protumoral microenvironment. Blood **2017**;129:1320-32
44. Zhang Y, Guo H, Zhang Z, Lu W, Zhu J, Shi J. IL-6 promotes chemoresistance via upregulating CD36 mediated fatty acids uptake in acute myeloid leukemia. Exp Cell Res **2022**;415:113112
45. Stavropoulou V, Kaspar S, Brault L, Sanders MA, Juge S, Morettini S*, et al.* MLL-AF9 Expression in Hematopoietic Stem Cells Drives a Highly Invasive AML Expressing EMT-Related Genes Linked to Poor Outcome. Cancer Cell **2016**;30:43-58
46. Montillo M, Tedeschi A, Rossi V, Cairoli R, Pungolino E, Intropido L*, et al.* Successful CD34+ cell mobilization by intermediate-dose Ara-C in chronic lymphocytic leukemia patients treated with sequential fludarabine and Campath-1H. Leukemia **2004**;18:57-62
47. Zhang T, Yang J, Vaikari VP, Beckford JS, Wu S, Akhtari M*, et al.* Apolipoprotein C2 - CD36 Promotes Leukemia Growth and Presents a Targetable Axis in Acute Myeloid Leukemia. Blood Cancer Discov **2020**;1:198-213
48. Moiseeva V, Cisneros A, Sica V, Deryagin O, Lai Y, Jung S*, et al.* Senescence atlas reveals an aged-like inflamed niche that blunts muscle regeneration. Nature **2023**;613:169-78
49. Chong M, Yin T, Chen R, Xiang H, Yuan L, Ding Y*, et al.* CD36 initiates the secretory phenotype during the establishment of cellular senescence. EMBO Rep **2018**;19
50. Perea G, Domingo A, Villamor N, Palacios C, Junca J, Torres P*, et al.* Adverse prognostic impact of CD36 and CD2 expression in adult de novo acute myeloid leukemia patients. Leuk Res **2005**;29:1109-16

TABLE 1 Multivariate analysis of the TUH cohort

		Haz. Ratio/ Robust SHR (CIR)	[95% Conf. Interval]	Std. Err.	z	P>|z|	Statistics
Event Free Survival (EFS)	**CD36**	1.55	**[1.174 - 2.051]**	0.22	3.09	0.002	**
	Age > 60 years	1.64	**[1.222 - 2.192]**	0.24	3.3	0.001	**
	WBC > 50G/L	1.85	**[1.314 - 2.591]**	0.32	3.54	0.000	***
	Allo-SCT	0.52	**[0.375 - 0.709]**	0.08	-4.09	0.000	***
	Favorable Cytogenetics	0.61	[0.361 - 1.03]	0.16	-1.85	0.064	ns
	Adverse Cytogenetics	1.34	[0.955 - 1.892]	0.23	1.7	0.090	ns
	FLT3-ITD mutation	1.31	[0.938 – 1.832]	0.22	1.59	0.113	ns
	NPM1 mutation	0.55	**[0.394 – 0.775]**	0.10	-3.43	0.001	**
	AML secondary status	1.53	**[1.134 – 2.06]**	0.23	2.78	0.005	**
Overall Survival (OS)	**CD36**	1.69	**[1.176 – 2.418]**	0.31	2.84	0.005	**
	Age > 60 years	1.39	[0.947 – 2.036]	0.27	1.68	0.093	ns
	WBC > 50G/L	1.84	**[1.192 – 2.833]**	0.41	2.76	0.006	**
	Allo-SCT	0.30	**[0.187 – 0.47]**	0.07	-5.17	0.000	***
	Favorable Cytogenetics	0.45	[0.203 – 1.003]	0.18	-1.95	0.051	ns
	Adverse Cytogenetics	1.41	[0.903 – 2.204]	0.32	1.51	0.131	ns
	FLT3-ITD mutation	1.46	[0.964 – 2.216]	0.31	1.79	0.074	ns
	NPM1 mutation	0.61	**[0.394 – 0.941]**	0.14	-2.23	0.026	*
	AML secondary status	1.85	**[1.272 – 2.697]**	0.36	3.22	0.001	***
Cumulative Incidence of Relapse (CIR)	**CD36**	1.53	**[1.07 – 2.193]**	0.28	2.33	0.020	*
	Age > 60 years	1.54	**[1.088 – 2.192]**	0.28	2.43	0.015	*
	WBC> 50G/L	1.57	**[1.008 – 2.458]**	0.36	1.99	0.046	*
	Allo-SCT	0.77	[0.519 – 1.128]	0.15	-1.35	0.177	ns
	Favorable Cytogenetics	0.76	[0.451 – 1.29]	0.20	-1.01	0.312	ns
	Adverse Cytogenetics	0.86	[0.524 – 1.424]	0.22	-0.57	0.566	ns
	FLT3-ITD mutation	1.19	[0.763 - 1.869]	0.27	0.78	0.437	ns
	NPM1 mutation	0.67	[0.437 - 1.014]	0.14	-1.9	0.058	ns
	AML secondary status	1.37	[0.921 - 2.05]	0.28	1.56	0.120	ns

Allo-SCT: Allogeneic stem-cell transplantation

WBC: White blood cells

FIGURE LEGENDS

Fig.1. CD36 expression in blasts at diagnosis is associated with human AML progression and relapse. a. AML patients from the TUH cohort (1273 patients) were classified as low and high CD36 expressers (CD36-expressing blasts <20%, Low, n=866 and CD36-expressing blasts ≥20%, High, n=407). **b**. Kaplan-Meier curve for even-free survival according to CD36 expression (CD36 Low n=298 and CD36 High n=136). **c**. Kaplan-Meier curve for overall survival according to CD36 expression (CD36 Low n=298 and CD36 High, n=136). **d.** Cumulative incidence of relapse according to CD36 expression (CD36 Low n=254, CD36 High, n=105). b, c, d. Log-Rank test. **e.** Box plot of CD36 expression on blasts according to cytogenetic risk (n=1191). Box plot shows the 10th percentile, first quartile, median, third quartile, and 90th percentile. Mann Whitney test was performed. **f.** Landscape of somatic mutations detected in diagnostic samples (n=224) by sequencing with a panel of 52 genes. The number of mutations for each patient is shown at the top, while the frequencies of each mutation are located at the right. **g.** Forrest plot showing mutation enrichment at AML diagnosis based on blast CD36 level by logarithmic odds ratio. Fisher's exact test was performed ($p = 0.029$ for FLT3). **h.** Forrest plot showing enrichment of recurrent cytogenetic anomalies at AML diagnosis according to CD36 expression by logarithmic odds ratio. Fisher's exact test was performed ($p < 0.0001$ for t(15;17) ; $p = 0.0008$ for t(9;22) ; $p = 0.0002$ for t(8;21) ; $p = 0.044$ for t(11q23;x)). The circles (in the center of the error bars) represent the odds ratios. The error bars represent 95% confidence interval of odds ratio.

Fig.2. CD36 inhibition delays AML relapse after chemotherapy. a. Percentage of mice engrafted with U937 cells transduced with shCtrl (n=11) or shCD36 (n=11) and treated with vehicle or AraC, surviving over time after treatment. **b.** Same as **a.** with OCIAML3 (shCtrl (n=18), shCD36 (n=22)). **c.** Percentage of mice engrafted with U937 cells surviving over time after treatment with the indicated combinations of PBS or AraC administered for the first 5 days, with either control IgG or FA6-152 anti-CD36 antibody injected 3 times/week (n=7 PBS-IGG, n=7 PBS-anti-CD36, n=7 AraC-IGG, n=6 AraC-anti-CD36). **d.** Venn diagram of significantly co-overexpressed genes along with CD36 in TCGA, Verhaak and BEATAML cohorts. **e.** GSEA of CD36 gene signature in AraC versus untreated AML blasts from 3 different transcriptomic analyses. a-c, log-rank (Mantel-Cox) test. e, one sample t test. *P<0.05, **P<0.01.

Fig.3. CD36 triggers blast migration. a. GO analysis of migration-related biological processes significantly enriched in the CD36 gene signature. **b**. Number of migrating shCtrl or shCD36 U937 cells in the lower chamber of the transwell assay (normalized to control) (n=5). **c.** As in **b.** but with CD36-blocking antibodies (FA6-152 or JC53.1) (n=4). **d.** Number of migrating cells in primary AML samples treated or not with CD36 blocking antibody (FA6-152) (n=7). **e.** Number of migrating shCtrl or shTSP1 U937 cells (normalized to control) (n=3). **f**. Number of migrating shCtrl or shCD36 U937 cells treated or not with TSP1-blocking antibody (A6.1) (normalized to shCtrl) (n=5). **g.** Number of migrating U937 cells treated or not with recombinant TSP1, in the presence or not of CD36-blocking antibody (FA6-152) (normalized to control) (n=3). **h**. As in **d.** but with TSP1-blocking antibody (A6.1) (n=5). **i.** Bioluminescence imaging of mice injected with the indicated AML cell line stably expressing a luciferase reporter from day 1 to day 64 after injection. **j.** Representative histological section showing anti-human Ku-80 labeling of U937 AML blasts in the subcutaneous adipose tissue 17 days post-xenograft. Positive brown nuclei highlight the infiltration of human blasts in murine adipose tissue either as dense infiltrate (left) or scattered isolated cells (right). Scale bar left image: 50µM, right image: 10µM. **k**. Percentage of viable OCIAML3 cells in the indicated tissues 14 days after orthotopic injection in the femur. **l.** Expression of CD36 (MFI) in viable OCIAML3 cells measured in the injected and contralateral femur and different organs of mice 14 days after orthotopic injection. Values are represented as mean ± SEM. b, c, e, one sample t test. d, h, paired t test. f, g ordinary one-way ANOVA with Tukey's multiple comparisons test. l, matched one-way ANOVA. *P<0.05, **P<0.01, ***P<0.001, ****P<0.0001.

Fig.4. Residual blasts maintained their migratory properties after chemotherapy. **a.** CD11b, CD14, CD15 and CD44 cell surface expression in viable control or AraC-treated (2 µM) U937 cells for 96h (n=4). **b.** GSEA of "HAY_BONE_MARROW_MONOCYTE" gene signature in AraC versus untreated AML samples from 3 different transcriptomic analyses. **c.** Number of migrating cells in the presence or absence of CD36-blocking antibody (FA6-152) sorted from control or 2 µM AraC treated cells for 4 days (normalized to control) (n=3). **d**. Percentage of viable CD36-low and CD36-high cells in PBS or 2µM AraC treated U937 cells for 4 days (n=4). **e.** Representative histograms of CD36 expression in non-migrating vs migrating CD36-low and CD36-high subpopulations sorted from control or AraC-treated U937 cells (2 µM) for 4 days. Plain histogram, non-migrating cells; striped histogram, migrating cells. **f.** Quantification of CD36 expression in non-migrating vs migrating cells in the same conditions as in **e.** (n = 3). **g.** Number of migrating cells from CD36-low and CD36-high subpopulations sorted from control or 2µM AraC treated U937 cells for 4 days (normalized to Ctrl CD36-low cells) (n=3). **h, i.** Quantification in the bone marrow (**h**) and spleen (**i**) of viable U937 cells transduced with shCtrl (n=9) or shCD36 (n=9) in mice relapsing after AraC treatment. **j-m.** Quantification of U937 cells by RT-qPCR (hCD45 mRNA normalized to m36B4) in SCAT (**j**), PGAT (**k**), lung (**l**) and kidneys (**m**) in mice relapsing after AraC treatment. Data expressed as $2^{-\Delta CT}$ (values multiplied by 1000) (n=4-5 shCtrl, n=5-7 shCD36). Values are represented as mean ± SEM. a, Mann-Whitney or unpaired t test depending on sample distribution. b, unpaired t test. c, g, ordinary one-way ANOVA with Tukey's multiple comparisons test. f, Ordinary two-way ANOVA with multiple comparisons correction. h-m, unpaired t test with or without Welch's correction depending on sample variance. *P<0.05, **P<0.01, ***P<0.001, ****P<0.0001.

Fig.5. Senescent-like state induced by cytarabine chemotherapy occurs specifically in CD36-high AML blasts. a, b. FSC/SCC analysis on gated CD36-low and CD36-high cells from U937 treated or not with 2µM AraC for 4 days (n=4). **c.** Representative histogram of C12FDG staining on gated CD36-low and CD36-high cells from U937 treated or not with 2µM AraC for 4 days. **d.** Quantification of C12FDG staining performed in **c**. (normalized to control CD36-low cells) (n=4). **e.** Expression of senescence-associated genes measured by RT-qPCR in CD36-low and CD36-high subpopulations sorted from control or 2µM AraC treated U937 cells for 4 days (normalized to Ctrl CD36-low cells). mRNA of the gene of interest normalized to the housekeeping gene, data expressed as 2ΔΔCt (n=4). **f.** C12FDG staining on U937 cells treated or not with 2µM AraC and CD36 blocking antibody (FA6-152) for 4 days. **g-m.** Expression of senescence-associated genes measured by RT-qPCR in 2µM AraC treated U937 cells with or without CD36 blocking antibody (FA6-152) for 4 days (normalized to AraC-treated cells). mRNA of the gene of interest normalized to the housekeeping gene, data expressed as 2ΔΔCt (n=5). Values are expressed as mean ± SEM. b, unpaired t test. d, e, f, ordinary one-way ANOVA with Tukey's multiple comparisons test. g-m, one sample Wilcoxon or t test depending on sample distribution. *P<0.05, **P<0.01, ***P<0.001.

Fig.6. Single-cell transcriptomic analysis reveals enrichment of CD36-high, migration and senescence-like gene signatures in a cluster emerging after standard chemotherapy. a. Schematic representation of the single-cell RNA-seq experiment performed on the TUH07 PDX previously published in Bosc et al. 2021 (GEO accession GSE178910). **b.** UMAP plot of 31,604 single cells from PDX TUH07 using Seurat. Colors indicate k-means clusters (k = 9). **c.** Cluster 8 was isolated on the Seurat object and bifurcated into two groups "CD36-High" and "CD36-Low" according to the enrichment level for the CD36 gene signature. Expression level of gene sets related to senescence (FRIDMAN_SENESCENCE_UP) and migration (WU_CELL_MIGRATION) are shown.

Fig.7. CD36 is positively associated with extramedullary disease in AML patients. a. Percentage of CD36+ blasts in the BM of patients with (LS+) or without (LS-) leukocytosis at diagnosis (n=596 LS-, n=46 LS+). **b.** Percentage of CD36+ blasts in the BM of patients presenting (EMD+, n=166) or not (EMD-, n=465) clinical signs of EMD at diagnosis. **c.** Percentage of CD36+ blasts in the BM of patients depending on the number of organs involved in EMD (n=465 for 0 organs, n=102 for 1 organ, n=45 for 2 organs, n=19 for more than 2 organs). **d.** Percentage of CD36+ blasts in the BM of patients at diagnosis, exhibiting MRD or not after chemotherapy (n=89 MRD-, n=67 MRD+). **e.** FSC/SCC analysis on blasts from CD36 low (n=12) and CD36 high (n=13) patients followed up from diagnosis to MRD. **f.** Cumulative incidence of relapse in TUH patients according to CD36 expression and presence of EMD at diagnosis (n=267). **g.** Overall survival in TUH patients according to CD36 expression and presence of EMD at diagnosis (n=319). Values are represented as mean ± SEM. a, b, d, Mann-Whitney test. C, ordinary one-way ANOVA with Tukey's multiple comparisons test. e, Wilcoxon matched-pairs signed rank test. f, g, Log-Rank test. *P<0.05, **P<0.01, ***P<0.001, ****P<0.0001.

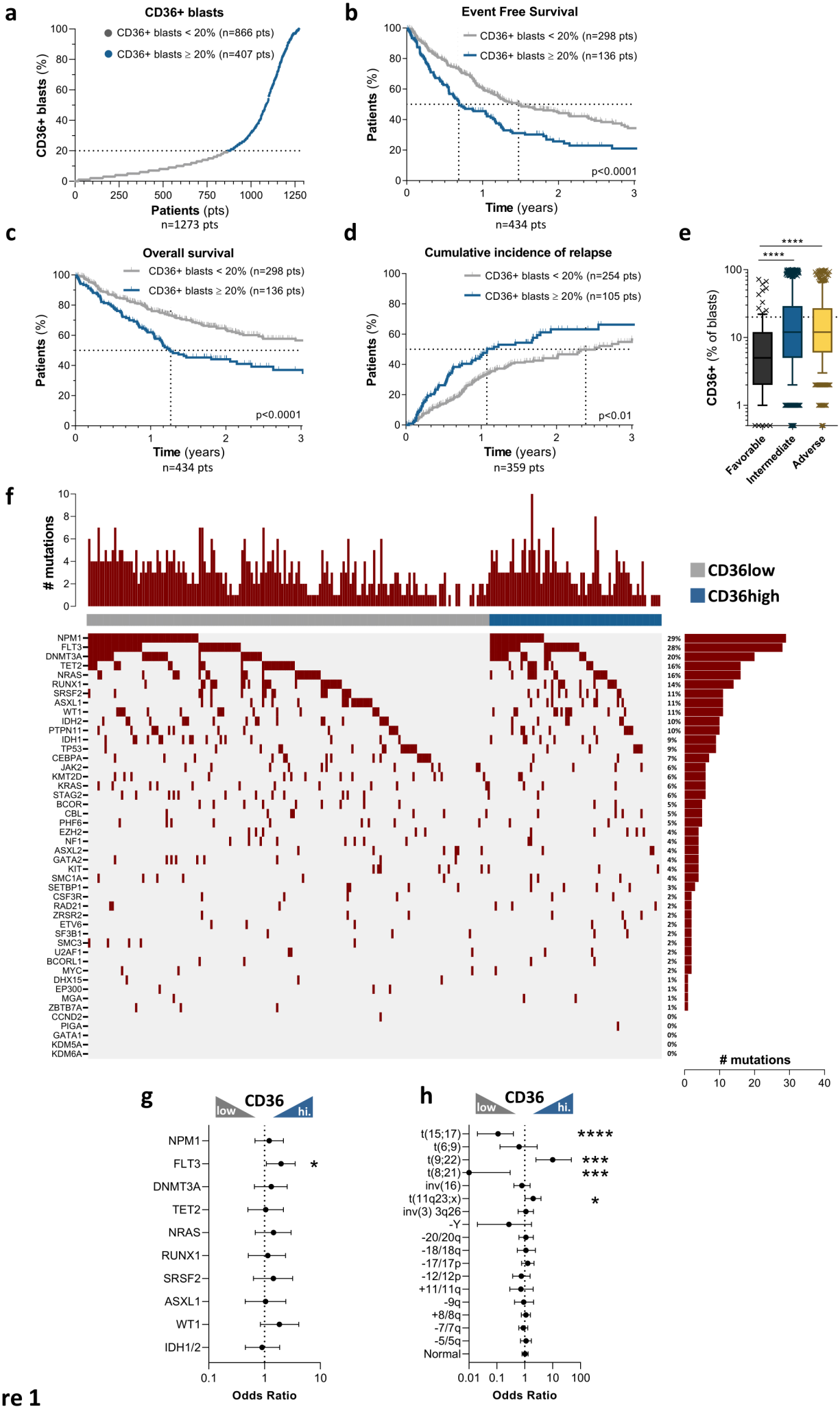
a
CD36+ blasts
CD36+ blasts < 20% (n=866 pts)
CD36+ blasts ≥ 20% (n=407 pts)
CD36+ blasts (%)
Patients (pts)
n=1273 pts
b
Event Free Survival
CD36+ blasts < 20% (n=298 pts)
CD36+ blasts ≥ 20% (n=136 pts)
Patients (%)
p<0.0001
Time (years)
n=434 pts
c
Overall survival
CD36+ blasts < 20% (n=298 pts)
CD36+ blasts ≥ 20% (n=136 pts)
Patients (%)
p<0.0001
Time (years)
n=434 pts
d
Cumulative incidence of relapse
CD36+ blasts < 20% (n=254 pts)
CD36+ blasts ≥ 20% (n=105 pts)
Patients (%)
p<0.01
Time (years)
n=359 pts
e
CD36+ (% of blasts)
****
****
Favorable
Intermediate
Adverse
f
mutations
CD36low
CD36high
NPM1 29%
FLT3 28%
DNMT3A 20%
TET2 16%
NRAS 16%
RUNX1 14%
SRSF2 11%
ASXL1 11%
WT1 11%
IDH2 10%
PTPN11 10%
IDH1 9%
TP53 9%
CEBPA 7%
JAK2 6%
KMT2D 6%
KRAS 6%
STAG2 6%
BCOR 5%
CBL 5%
PHF6 5%
EZH2 4%
NF1 4%
ASXL2 4%
GATA2 4%
KIT 4%
SMC1A 4%
SETBP1 3%
CSF3R 2%
RAD21 2%
ZRSR2 2%
ETV6 2%
SF3B1 2%
SMC3 2%
U2AF1 2%
BCORL1 2%
MYC 2%
DHX15 1%
EP300 1%
MGA 1%
ZBTB7A 1%
CCND2 0%
PIGA 0%
GATA1 0%
KDM5A 0%
KDM6A 0%
mutations
g
CD36
low
hi.
NPM1
FLT3 *
DNMT3A
TET2
NRAS
RUNX1
SRSF2
ASXL1
WT1
IDH1/2
Odds Ratio
h
CD36
low
hi.
t(15;17) ****
t(6;9)
t(9;22) ***
t(8;21) ***
inv(16)
t(11q23;x) *
inv(3) 3q26
-Y
-20/20q
-18/18q
-17/17p
-12/12p
+11/11q
-9q
+8/8q
-7/7q
-5/5q
Normal
Odds Ratio

Figure 1

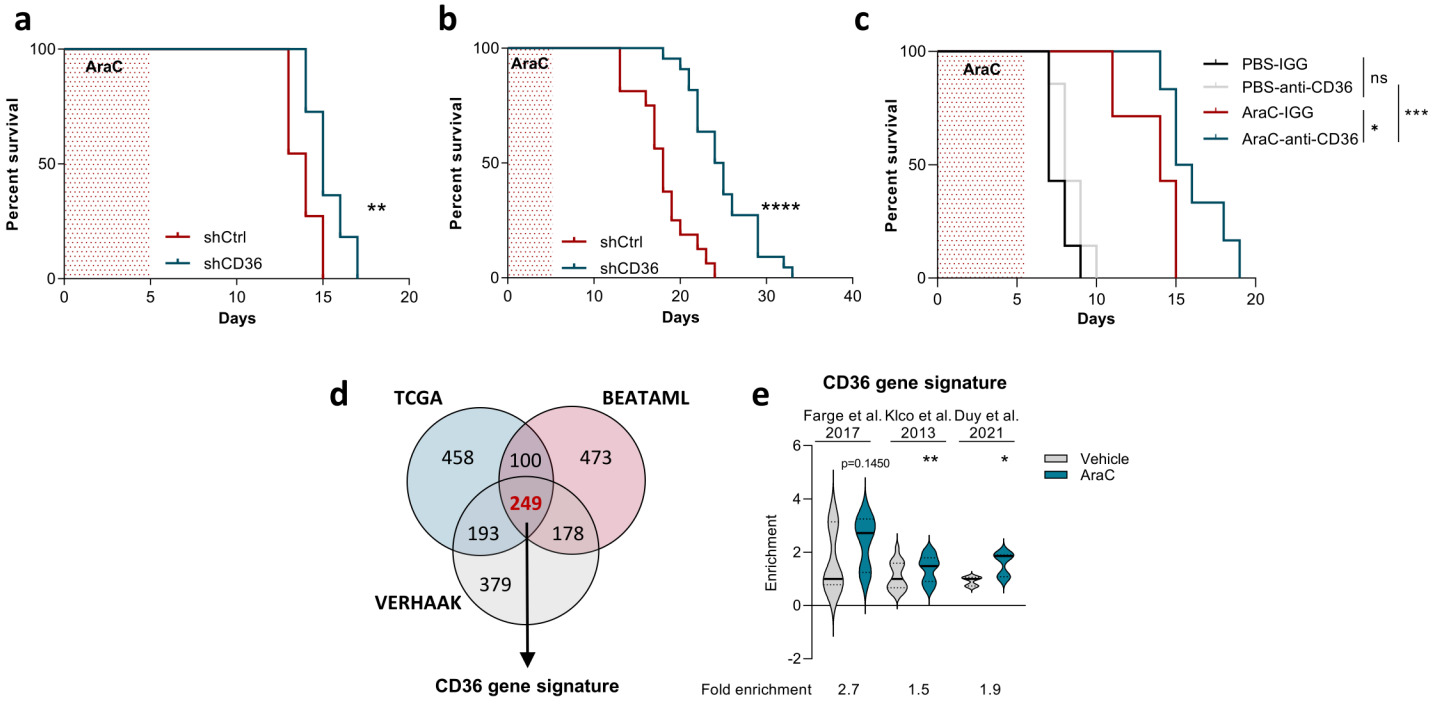
a
b
c
AraC
Percent survival
Days
shCtrl
shCD36
**
****
PBS-IGG
PBS-anti-CD36
AraC-IGG
AraC-anti-CD36
ns
*
***
d
TCGA
BEATAML
VERHAAK
458
100
473
249
193
178
379
CD36 gene signature
e
CD36 gene signature
Farge et al. 2017
Klco et al. 2013
Duy et al. 2021
p=0.1450
**
*
Vehicle
AraC
Enrichment
Fold enrichment
2.7
1.5
1.9

Figure 2

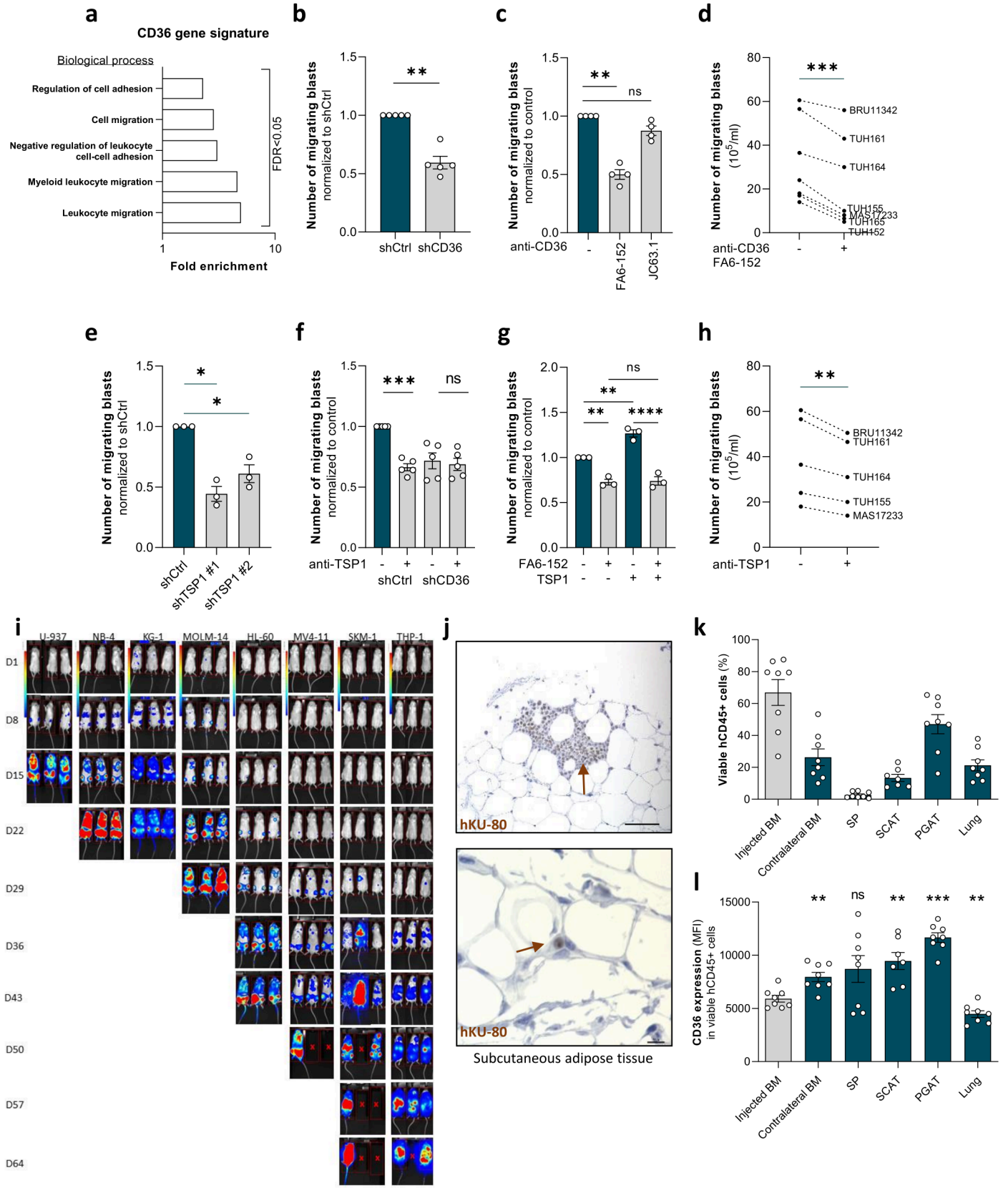
a
CD36 gene signature
Biological process
Regulation of cell adhesion
Cell migration
Negative regulation of leukocyte cell-cell adhesion
Myeloid leukocyte migration
Leukocyte migration
FDR<0.05
1
10
Fold enrichment
b
Number of migrating blasts normalized to shCtrl
shCtrl
shCD36
c
Number of migrating blasts normalized to control
anti-CD36
FA6-152
JC63.1
d
Number of migrating blasts (10^5/ml)
BRU11342
TUH161
TUH164
TUH155
MAS17233
TUH165
TUH152
anti-CD36
FA6-152
e
Number of migrating blasts normalized to shCtrl
shCtrl
shTSP1 #1
shTSP1 #2
f
Number of migrating blasts normalized to control
anti-TSP1
shCtrl
shCD36
g
Number of migrating blasts normalized to control
FA6-152
TSP1
h
Number of migrating blasts (10^5/ml)
BRU11342
TUH161
TUH164
TUH155
MAS17233
anti-TSP1
i
U-937
NB-4
KG-1
MOLM-14
HL-60
MV4-11
SKM-1
THP-1
D1
D8
D15
D22
D29
D36
D43
D50
D57
D64
j
hKU-80
hKU-80
Subcutaneous adipose tissue
k
Viable hCD45+ cells (%)
Injected BM
Contralateral BM
SP
SCAT
PGAT
Lung
l
CD36 expression (MFI) in viable hCD45+ cells
Injected BM
Contralateral BM
SP
SCAT
PGAT
Lung

Figure 3

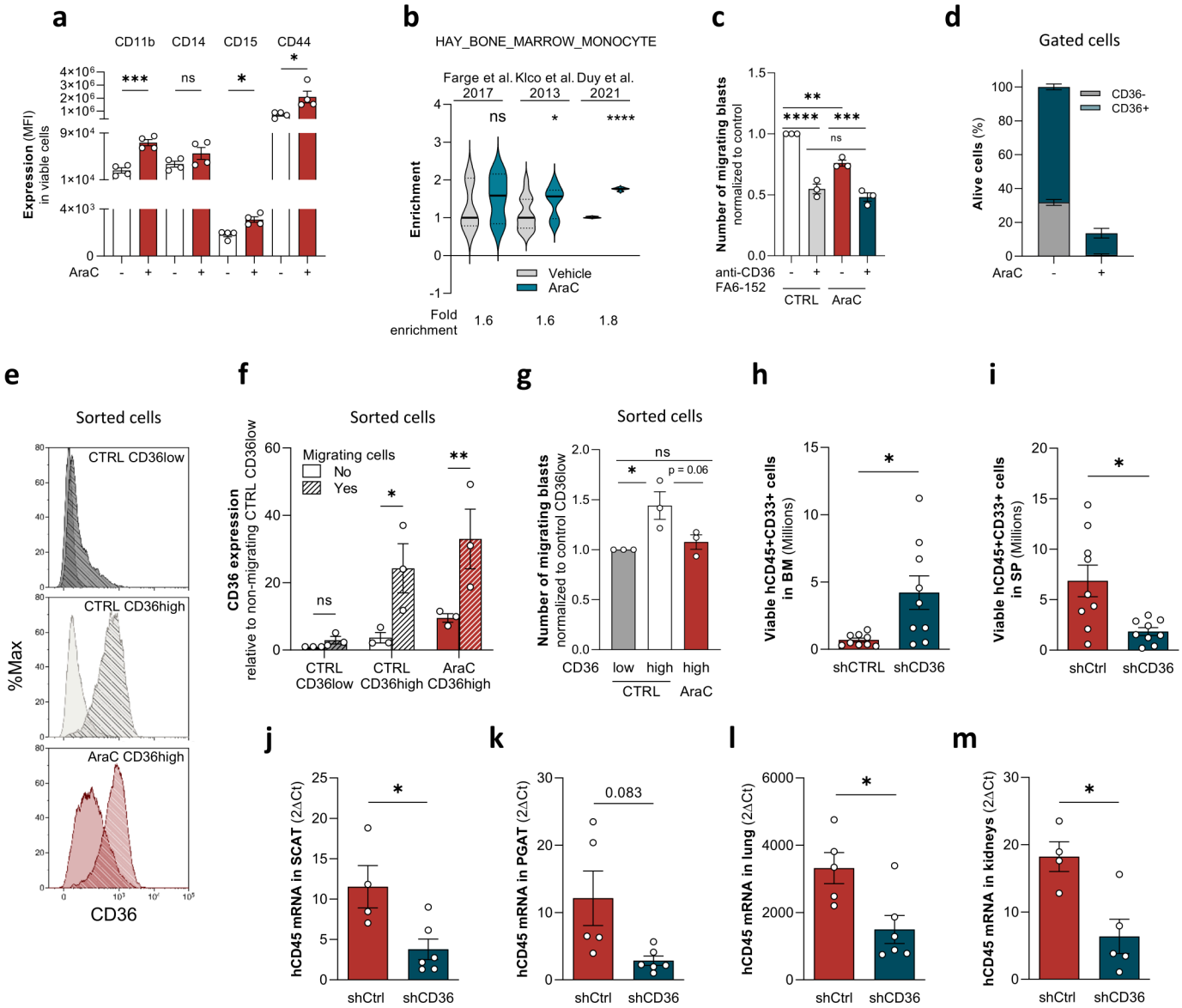
a
CD11b
CD14
CD15
CD44
Expression (MFI) in viable cells
AraC
b
HAY_BONE_MARROW_MONOCYTE
Farge et al. 2017
Klco et al. 2013
Duy et al. 2021
Enrichment
Vehicle
AraC
Fold enrichment
1.6
1.6
1.8
c
Number of migrating blasts normalized to control
anti-CD36
FA6-152
CTRL
AraC
d
Gated cells
Alive cells (%)
CD36-
CD36+
AraC
e
Sorted cells
CTRL CD36low
CTRL CD36high
AraC CD36high
%Max
CD36
f
Sorted cells
CD36 expression relative to non-migrating CTRL CD36low
Migrating cells
No
Yes
CTRL CD36low
CTRL CD36high
AraC CD36high
g
Sorted cells
Number of migrating blasts normalized to control CD36low
p = 0.06
CD36
low
high
high
CTRL
AraC
h
Viable hCD45+CD33+ cells in BM (Millions)
shCTRL
shCD36
i
Viable hCD45+CD33+ cells in SP (Millions)
shCtrl
shCD36
j
hCD45 mRNA in SCAT (2ΔCt)
shCtrl
shCD36
k
hCD45 mRNA in PGAT (2ΔCt)
0.083
shCtrl
shCD36
l
hCD45 mRNA in lung (2ΔCt)
shCtrl
shCD36
m
hCD45 mRNA in kidneys (2ΔCt)
shCtrl
shCD36

Figure 4

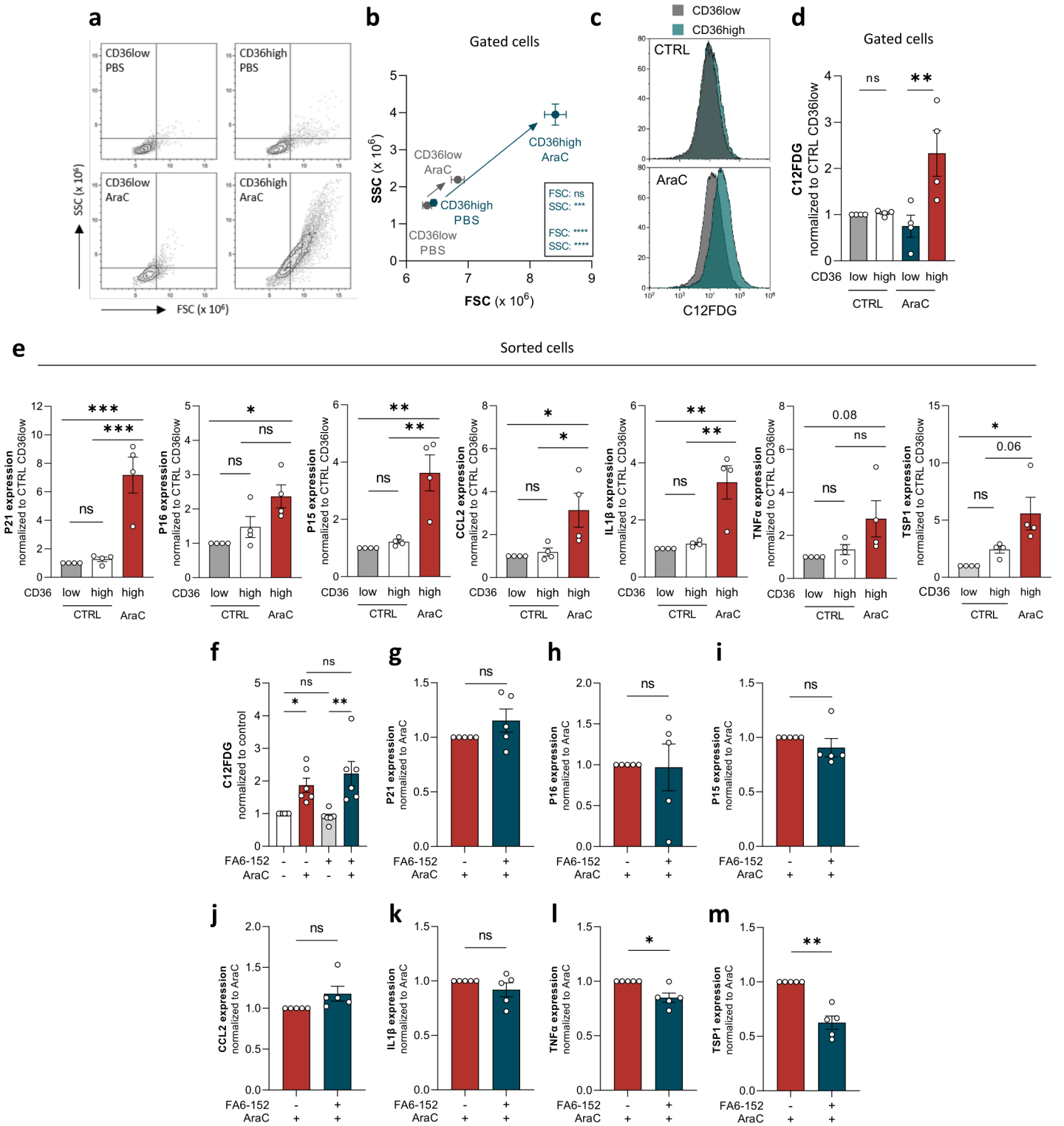
a
CD36low PBS
CD36high PBS
CD36low AraC
CD36high AraC
SSC (x 10⁶)
FSC (x 10⁶)
b
Gated cells
CD36low AraC
CD36high AraC
CD36high PBS
CD36low PBS
FSC: ns
SSC: ***
FSC: ****
SSC: ****
SSC (x 10⁶)
FSC (x 10⁶)
c
CD36low
CD36high
CTRL
AraC
C12FDG
d
Gated cells
C12FDG normalized to CTRL CD36low
ns
**
CD36 low high low high
CTRL AraC
e
Sorted cells
P21 expression normalized to CTRL CD36low
P16 expression normalized to CTRL CD36low
P15 expression normalized to CTRL CD36low
CCL2 expression normalized to CTRL CD36low
IL1β expression normalized to CTRL CD36low
TNFα expression normalized to CTRL CD36low
TSP1 expression normalized to CTRL CD36low
CD36 low high high
CTRL AraC
f
C12FDG normalized to control
FA6-152
AraC
g
P21 expression normalized to AraC
h
P16 expression normalized to AraC
i
P15 expression normalized to AraC
j
CCL2 expression normalized to AraC
k
IL1β expression normalized to AraC
l
TNFα expression normalized to AraC
m
TSP1 expression normalized to AraC

Figure 5

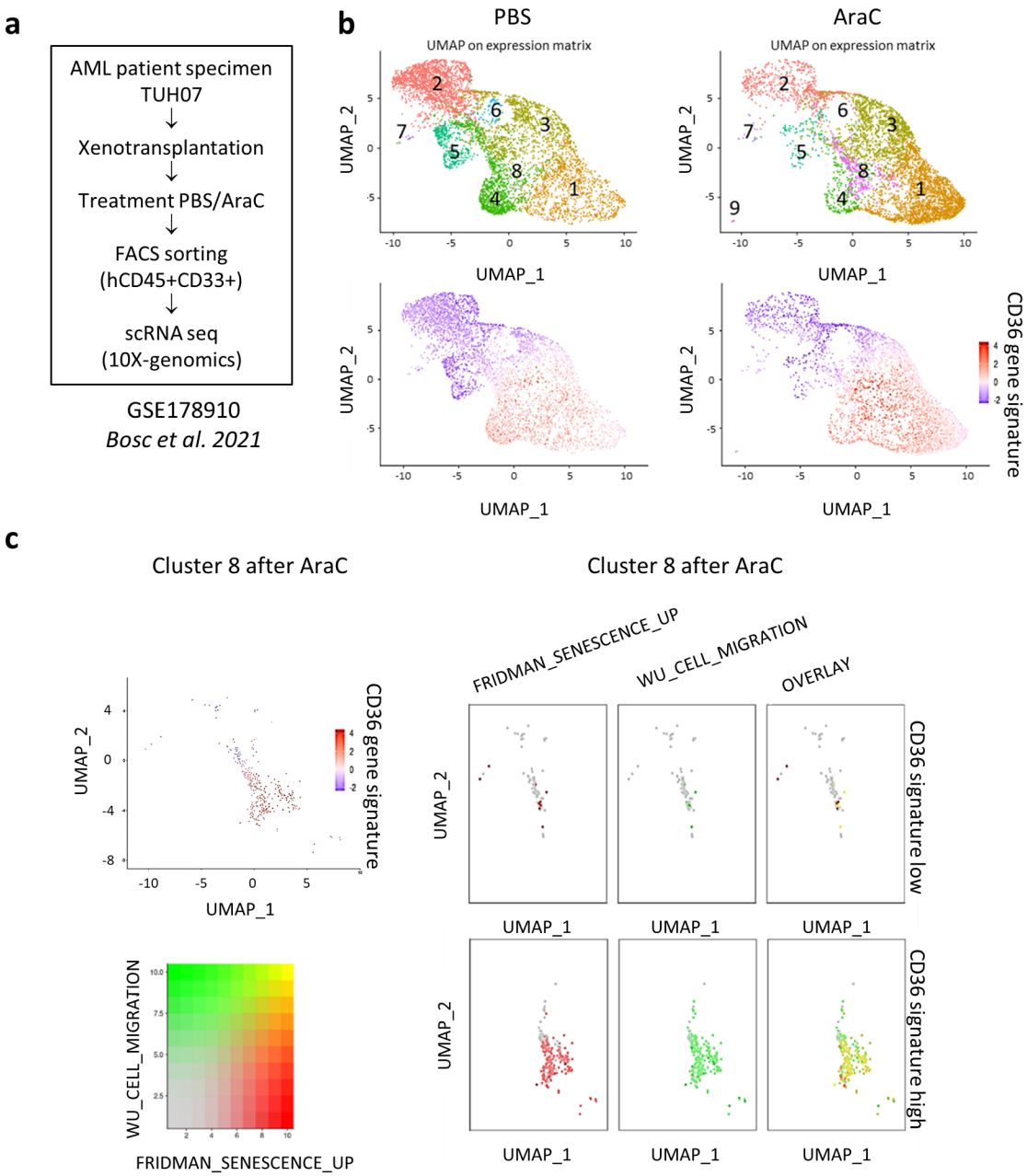
a
AML patient specimen
TUH07
Xenotransplantation
Treatment PBS/AraC
FACS sorting
(hCD45+CD33+)
scRNA seq
(10X-genomics)
GSE178910
Bosc et al. 2021
b
PBS
AraC
UMAP on expression matrix
UMAP_1
UMAP_2
CD36 gene signature
c
Cluster 8 after AraC
Cluster 8 after AraC
FRIDMAN_SENESCENCE_UP
WU_CELL_MIGRATION
OVERLAY
CD36 signature low
CD36 signature high

Figure 6

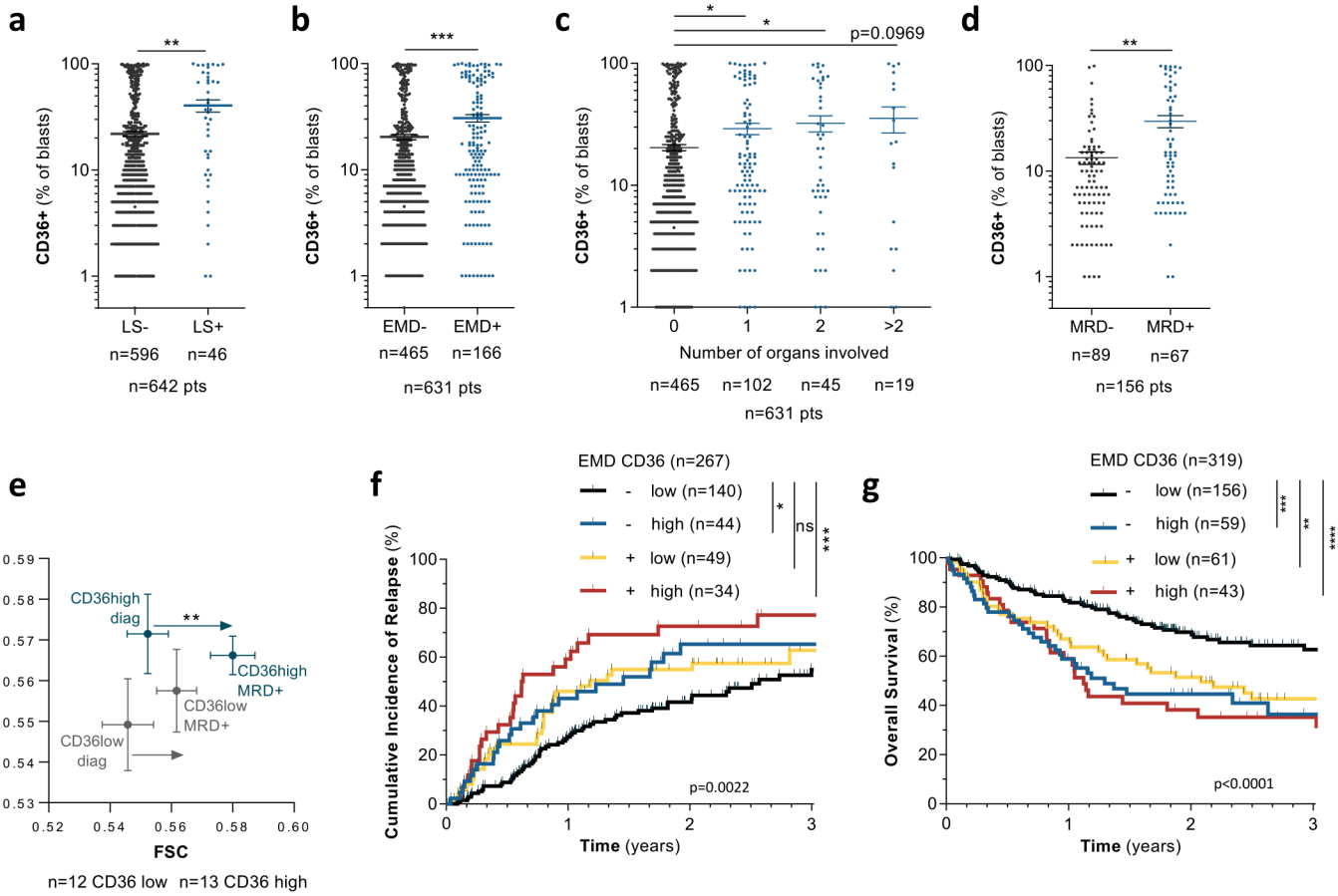
a
b
c
d
CD36+ (% of blasts)
LS-
LS+
n=596
n=46
n=642 pts
EMD-
EMD+
n=465
n=166
n=631 pts
p=0.0969
0
1
2
>2
Number of organs involved
n=465
n=102
n=45
n=19
n=631 pts
MRD-
MRD+
n=89
n=67
n=156 pts
e
SSC
FSC
CD36high diag
CD36high MRD+
CD36low MRD+
CD36low diag
n=12 CD36 low
n=13 CD36 high
f
EMD CD36 (n=267)
- low (n=140)
- high (n=44)
+ low (n=49)
+ high (n=34)
Cumulative Incidence of Relapse (%)
Time (years)
p=0.0022
ns
g
EMD CD36 (n=319)
- low (n=156)
- high (n=59)
+ low (n=61)
+ high (n=43)
Overall Survival (%)
Time (years)
p<0.0001

Figure 7

SUPPLEMENTAL MATERIALS

CD36 drives metastasis and relapse in acute myeloid leukemia

Thomas Farge[1,2,3,4,5,6†], Jean Nakhle[6†], Damien Lagarde[6,7,8], Guillaume Cognet[1,2,3], Nathaniel Polley[1,2,3], Rémy Castellano[9], Marie-Laure Nicolau[10,11], Claudie Bosc[1,2,3], Marie Sabatier[1,2,3], Ambrine Sahal[1,2,3], Estelle Saland[1,2,3], Yannick Jeanson[6], Nathan Guiraud[1,2,3], Emeline Boet[1,2,3], Camille Bergoglio[12], Mathilde Gotanègre[1,2,3], Pierre-Luc Mouchel[1,2,3,10,11], Lucille Stuani[1,2,3], Clément Larrue[1,2,3], Marie Sallese[6], Véronique De Mas[1,2,3,10,11], Cedric Moro[12], Cédric Dray[6], Yves Collette[9], Isabelle Raymond-Letron[6,13], Isabelle Ader[6], Christian Récher[1,2,3,10,11], Jean-Emmanuel Sarry [1,2,3], Florence Cabon[1,2,3‡], François Vergez[1,2,3,10,11‡], and Audrey Carrière[6‡*]

[1]Centre de Recherches en Cancérologie de Toulouse, Université de Toulouse, Inserm, CNRS, Toulouse, France.
[2]LabEx Toucan, Toulouse, France.
[3]Equipe Labellisée Ligue Nationale Contre le Cancer 2023, Toulouse, France.
[4]Institute of Metabolic and Cardiovascular Diseases, Team CERAMIC, INSERM, Paul Sabatier University, UMR1297, Toulouse, France
[5]Institut Fédératif de Biologie (IFB), CHU Toulouse, Toulouse, France
[6]RESTORE Research Center, Université de Toulouse, INSERM 1301, CNRS 5070, EFS, ENVT, Toulouse, France
[7]McGill University, Rosalind and Morris Goodman Cancer Institute, Montréal, Québec, Canada
[8]McGill University, Department of Biochemistry, Montréal, Québec, Canada
[9]Centre de Recherche en Cancérologie de Marseille, Aix-Marseille Univ, Inserm, CNRS, Institut Paoli-Calmettes, 13009 Marseille, France
[10]University of Toulouse, Toulouse, France.
[11]Centre Hospitalier Universitaire de Toulouse, Institut Universitaire du Cancer de Toulouse Oncopole, Service d'Hématologie, Université Toulouse III Paul Sabatier, Toulouse, France.
[12]Institute of Metabolic and Cardiovascular Diseases, Team MetaDiab, INSERM, Paul Sabatier University, UMR1297, Toulouse, France
[13]LabHPEC, Université de Toulouse, ENVT, Toulouse, France

† These authors contributed equally to this work

‡ These authors jointly supervised this work

* Corresponding author. Audrey Carrière, RESTORE Research Center, Bâtiment INCERE, 4bis avenue Hubert Curien, 31000 Toulouse, audrey.carriere-pazat@inserm.fr

Short running title: CD36-dependent metastasis in acute myeloid leukemia

Conflict of interest: The authors declare no conflict of interest.

Keywords: acute myeloid leukemia, metastasis, CD36

MATERIAL AND METHODS

Cell lines, primary cultures, and culture conditions

Primary AML cells, peripheral blood or bone marrow patients' samples were frozen in FCS with 10% DMSO and stored in liquid nitrogen. The percentage of blasts was determined by flow cytometry and morphologic characteristics before purification. Cells were thawed at 37 °C, washed in thawing media composed of IMDM, 20% FBS. Cells were maintained in IMDM, 20% FBS, and 1% Pen/Strep (GIBCO) for all experiments.

Human AML cell lines were maintained in MEMa-media (Gibco) supplemented with 10% FBS (Invitrogen) in the presence of 100 U/ml of penicillin and 100 µg/ml of streptomycin, and were incubated at 37 °C with 5% CO2. Cells were split every 2–3 days and maintained in an exponential growth phase. All AML cell lines were purchased at DSMZ or ATCC. These cell lines have been routinely tested for Mycoplasma contamination in the laboratory. The U937 cells were obtained from the DSMZ in February 2012 and from the ATCC in January 2014.

Bioluminescent xenograft mouse models

Briefly, 6 to 10-week-old NOD.Cg-Prkdc scid/J (NSG) mice were obtained from Charles River France or bred in-house and maintained on a 12-h light and 12-h dark cycle, under specific pathogen-free conditions with sterilized food and water provided ad libitum. Animals were injected via tail vein at day 0 with 0.2x106 viable luciferase-expressing AML cell lines in 0.1mL sterile PBS. A bioluminescence measurement was performed at day 1, then once a week, following injection of endotoxin-free luciferin (Promega #E6552, 30 mg/kg) using an Optima PhotonIMAGER imaging system and analyzed using M3vision software (Biospace Lab, Nesles-la-Vallée, France). Daily monitoring of mice for symptoms of disease (weight loss >20%, ruffled coat, hunched back, weakness, reduced motility) determined the time of killing for injected animals with signs of distress. After the final time point, for ex vivo organ imaging, 10 min after receiving luciferin, mice were killed and organs were collected and washed with PBS. Images were then immediately acquired in indicated organs. Results were expressed as percentage of total signal (100*(organ signal/total bioluminescence).

Assessment of leukemic engraftment

At the end of the experiment, NSG mice were humanely killed in accordance with European ethics protocol. Bone marrow (mixed from tibias and femurs), spleen and liver were dissected and flushed in HBSS with 1% FBS. Mononuclear cells from bone marrow and spleen were labeled with anti-hCD33, anti-mCD45.1, anti-hCD45, anti-hCD3, and/or anti-hCD44 (all from BD) antibodies to determine the fraction of viable human blasts (hCD3−hCD45+mCD45.1−hCD33+/hCD44+AnnV− cells) by flow cytometry. Adipose tissues and lungs were dissociated with collagenase NB4 (Standart Grade from Coger) 0.4 U/mL for 30 minutes. Acquisitions were performed on a CytoFLEX flow cytometer with CytoExpert software v2.0 (Beckman Coulter), and analyses done with Flowjo v10.4.2. The number of AML cells/µL of peripheral blood and number of AML cells in total leukemia burden (in bone marrow, spleen, subcutaneous and perigonadic adipose tissues, liver and lungs) were determined using CountBright beads (Invitrogen) as described in the provided protocol.

Single cell analysis

Next generation sequencing of single cell gene expression (NextSeq 550) was performed on each of the two experimental groups (vehicle or AraC) of the PDX patient TUH07 (GEO accession GSE178910) published in (1), to produce raw FASTQ reads. Gene expression data had been rendered from FASTQ reads using CellRanger software by 10x Genomics. The quality control, principle component analysis (PCA), and t-SNE/UMAP dimensionality reduction procedures to integrate and visualize the scRNAseq expression data of the patients was performed using R package Seurat 3.0 by Satija Lab. The corresponding input parameters and functional R scripts to execute the aforementioned procedures are publicly available on the Zenodo repository (accession 5137701). Cells were classified into their corresponding clusters on a UMAP projection based upon their phenotypic characteristic at diagnosis and response to therapies. Clusters significantly increasing in cell count after Arac treatment in proportion to the entire cell population were considered “enriched”, while clusters that significantly decreased in cell count were considered “sensitive”. A standard Z-test for difference in proportions had

been utilized to facilitate this classification and determine the statistical significance of each change in cluster size according to its calculated z-value (**Table S2**).

In order to assign enrichment values to the metadata of the single-cell samples, the Seurat function "AddModuleScore" had been implemented for the gene expression signatures: CD36, FRIDMAN_SENESCENCE_UP, and WU_MIGRATION (**Table S2**) with the "search" parameter set as "TRUE". The enrichment values pertaining to each cell were z-standardized using the base-R "scale" function.

To visualize the enrichment regions of the aforementioned gene expression signatures, the method "FeaturePlot" was used on the PDX category subset by patient number and treatment type. To maintain visual continuity across each FeaturePlot, the maximum and minimum z-scores for the color gradient were standardized to the 0.999 and 0.001 percentile expression values respectively in order to mitigate the effect of outliers. For the correlation analyses performed among the gene expression signatures at the cellular level, the function "FeatureScatter" had been implemented to both derive linear Pearson correlation coefficients (r) and to visualize the effect of each individual cluster on the overall relationship between the variables examined. Differential CD36 signature expression was derived for each cluster using the "col_t_welch" function from the matrixTests R library, which produced the relevant test statistics for a two-sample t-test of unpaired means for different variances (**Table S2**). The same process was then performed for senescence and migratory signatures (**Table S2**).

The cluster 8 was isolated using base-R command "subset" (with parameter 'subset = "seurat_clusters" == 8') on the Seurat object belonging to patient TUH07-AraC. To better assess the overlapping effects of CD36 with senescence and migration within this cluster, it had been bifurcated into two groups "CD36 High" and "CD36 Low" by assigning a new "CD36" field to the cluster's Seurat metadata. Using the base-R "ifelse" function, all cells with z-scores greater than zero in CD36 signature expression were assigned "CD36 High", and cells having less than z = 0 were assigned "CD36 Low" and recorded on the "CD36" metadata field. To facilitate the rendering of the blended plot visualizing the overlap of senescence and migratory activity exclusive to the CD36 enrichment within cluster 8, the "FeaturePlot" Seurat function was utilized with its functions: "blend = TRUE", "features = c("FRIDMAN_SENESCENCE_UP", "WU_CELL_MIGRATION")", and "split.by = "CD36"".

GSEA analysis

GSEA analysis was performed using GSEA version 4.0 (Broad Institute). Gene signatures used in this study were from Broad Institute database, literature, or in-house built. Following parameters were used: Number of permutations = 1000, permutation type = gene_set. Other parameters were left at default values.

Plasmid cloning, shRNA, lentiviral production, and leukemic cell transduction

Control shRNA (MFCD07785395), CD36 shRNA (TRCN0000056998) and TSP1 shRNA plasmids (TRCN0000226405 and TRCN0000219072) on a pLKO.1 backbone were purchased from Sigma. shRNA, lentiviral production and cell transduction was performed as previously described (2).

SA-β-gal activity measurement by C12-FDG staining

C12-FDG staining was performed as previously (3). Briefly, cells were treated with 100 nM Bafilomycin A1 (Invivogen tlrl-bafa1) for 2 hours then incubated with 20 µM C12-FDG (Abcam ab273642) in the dark for 1 hour at 37 °C. Cells were then washed with PBS and stained for flow cytometry as per usual.

Number of viable cells

U937 and OCIAML3 cells (300,000/mL) were seeded for 72-96h in MEMa-media (Gibco) supplemented with 10% FBS (Invitrogen) in the presence of 100 U/ml of penicillin and 100 µg/ml of streptomycin, and diluted in half with fresh media at 48h. Two technical replicated were seeded in a 24-well plate for each condition. Alive cells were counted every 24h on a Malassez chamber using Trypan Blue staining.

Primers

Primers sequences are : CCL2 (human) Forward - CATGAAAGTCTCTGCCGCCC and Reverse - GGGGCATTGATTGCATCTGGC), **P21 (human)** Forward - TGCCGAAGTCAGTTCCTTGT and Reverse - GTTCTGACATGGCGCCTCC; **P16 (human)** Forward - GGGGTCGGGTAGAGGAGG and Reverse - GCCCATCATCATGACCTGGA; **P15 (human)** Forward -

GGGACTAGTGGAGAAGGTGC and Reverse - CCATCATCATGACCTGGATCG; **IL1-β (human)** - Forward - AGCCATGGCAGAAGTACCTG and Reverse - CCTGGAAGGAGCACTTCATCT; **TNF-α (human)** - Forward - GCCCATGTTGTAGCAAACCC and Reverse - TATCTCTCAGCTCCACGCCA; **TSP1 (human)** - Forward - CTCAGGACCCATCTATGATAAAACC and Reverse - AAGAAGGAAGCCAAGGAGAAGTG; **CD45 (human)** Forward - CACTGCAGGGATGGATCTCA and Reverse - TGCGTAGAGCTTTTACCACTTGAA; **RPLP0 (human)** Forward - TAGTTGGACTTCCAGGTCGC and Reverse - CGTCCTCGTGGAAGTGACAT and **36b4 (mouse)** Forward - AGTCGGAGGAATCAGATGAGGAT and Reverse - GGCTGACTTGGTTGCTTTGG.

Molecular analysis

The presence of *FLT3-ITD* was tested as described (4). Electrophoregram peaks were quantified using GeneMarker 2.2 (SoftGenetics, State College, PA). Extended DNA resequencing was performed using Illumina NextSeq500 and Haloplex HS (Agilent, Santa Clara, CA) targeted on the complete coding regions of 52 genes: *ASXL1*, *ASXL2*, *ATM*, *BCOR*, *BCORL1*, *CBL*, *CCND2*, *CEBPA*, *CSF3R*, *CUX1*, *DDX41*, *DHX15*, *DNMT3A*, *EP300*, *ETV6*, *EZH2*, *FLT3*, *GATA1*, *GATA2*, *IDH1*, *IDH2*, *JAK2*, *KDM5A*, *KDM6A*, *KIT*, *KMT2D*, *KRAS*, *MGA*, *MPL*, *MYC*, *NF1*, *NPM1*, *NRAS*, *PHF6*, *PIGA*, *PPM1D*, *PRPF8*, *PTPN11*, *RAD21*, *RUNX1*, *SETBP1*, *SF3B1*, *SMC1A*, *SMC3*, *SRSF2*, *STAG2*, *TET2*, *TP53*, *U2AF1*, *WT1*, *ZBTB7A*, and *ZRSR2*. Data were processed through two algorithms from GATK (https://software.broadinstitute.org/gatk), HaplotypeCaller (scaling accurate genetic variant discovery) to tens of thousands of samples (5). The mean depth was 2,190 reads. Identified variants were curated manually and named according to the rules of the Human Genome Variation Society (hgvs.org). Molecular data are stored in the European Nucleotide Archive (https://www.ebi.ac.uk/ena/).

References

1. Bosc C, Saland E, Bousard A, Gadaud N, Sabatier M, Cognet G*, et al.* Mitochondrial inhibitors circumvent adaptive resistance to venetoclax and cytarabine combination therapy in acute myeloid leukemia. Nat Cancer **2021**;2:1204-23
2. Larrue C, Guiraud N, Mouchel PL, Dubois M, Farge T, Gotanegre M*, et al.* Adrenomedullin-CALCRL axis controls relapse-initiating drug tolerant acute myeloid leukemia cells. Nat Commun **2021**;12:422
3. Debacq-Chainiaux F, Erusalimsky JD, Campisi J, Toussaint O. Protocols to detect senescence-associated beta-galactosidase (SA-betagal) activity, a biomarker of senescent cells in culture and in vivo. Nat Protoc **2009**;4:1798-806

4. Largeaud L, Cornillet-Lefebvre P, Hamel JF, Dumas PY, Prade N, Dufrechou S*, et al.* Lomustine is beneficial to older AML with ELN2017 adverse risk profile and intermediate karyotype: a FILO study. Leukemia **2021**;35:1291-300
5. McKenna A, Hanna M, Banks E, Sivachenko A, Cibulskis K, Kernytsky A*, et al.* The Genome Analysis Toolkit: a MapReduce framework for analyzing next-generation DNA sequencing data. Genome Res **2010**;20:1297-303

SUPPLEMENTAL FIGURES

Fig. S1. Characterization of CD36 role in lipid metabolism in blasts. a-d. Cell surface CD36 expression (**a, b**) of viable human AML blasts in the BM of vehicle- or AraC-treated AML PDX. **c**. Representative flow cytometry histograms of basal CD36 expression in U937 and OCIAML3 cells. **d.** CD36 protein expression in AML cells treated with AraC for 24h, relative to that of PBS-treated cells. AraC concentrations used were 2µM for U937 and 10µM for OCIAML3 cells (n=5). **e-f.** Viable cell number of shCtrl and shCD36 U937 (**e**) and OCIAML3 (**f**) cells proliferating over 72h (n=4). **g-h.** Viable cell number of U937 (**g**) and OCIAML3 (**h**) cells proliferating over 96h in the presence of FA6-152 antiCD36 antibody (0-10 µg/ml) (n=3). **i**. Representative flow cytometry histograms of CD36 expression in shCtrl and shCD36 U937 cells treated with vehicle or 2µM AraC for 24h. **j-k.** CD36 expression assessed by flow cytometry in shCtrl or shCD36 cells treated with vehicle or AraC (2µM for U937 (**j**), 10µM for OCIAML3 (**k**)) for 24h (n=4-6). Values are normalized to control. **l-m.** Neutral lipid staining measured by flow cytometry using the Bodipy probe, in viable shCtrl or shCD36 U937 (**l**) and OCIAML3 (**m**) cells treated with vehicle or AraC (2µM for U937, 10µM for OCIAML3) for 24h (n=3-4). Values are normalized to control. **n-o.** Neutral lipid content measured by flow cytometry using the Bodipy probe, in viable U937 treated with vehicle or AraC (2µM) and/or CD36 blocking antibody (JC63.1, (**n**) or FA6-152 (**o**) for 24h (n=3-4). Values are normalized to control. **p.** Representative flow cytometry histograms of CD36 expression in siCtrl and siCD36 U937 cells treated with vehicle or 2µM AraC for 24h. **q.** CD36 expression in siCtrl and siCD36 U937 cells treated with vehicle or 2µM AraC for 24h (n=4). Values are normalized to control. **r, s.** 14C palmitate uptake **(r)** and oxidation **(s)** in siCtrl and siCD36 U937 cells treated with vehicle or AraC (2µM) for 24h (n=4). Values are normalized to the number of viable cells per condition and reported as a fold change to control. **t-u.** 14C palmitate uptake **(t)** and oxidation **(u)** in U937 cells treated with vehicle or AraC (2µM) and/or CD36 blocking antibody (FA6-152) for 24h (n=4). Values are normalized to the number of viable cells per condition and reported as a fold change to control. **v.** Representative flow cytometry histograms of CD36 expression in siCtrl and siCD36 OCIAML3 cells treated with vehicle or 2µM AraC for 24h. **w.** CD36 expression in siCtrl and siCD36 OCIAML3 cells treated with vehicle or 10µM AraC for 24h (n=4). Values are normalized to control. **x-y.** 14C palmitate uptake **(x)** and oxidation **(y)** in siCtrl and siCD36 OCIAML3 cells treated

with vehicle or AraC (10μM) for 24h (n=4). Values are normalized to the number of viable cells per condition and reported as a fold change to control. **z-aa.** 14C palmitate uptake **(z)** and oxidation **(aa)** in OCIAML3 cells treated with vehicle or AraC (10μM) and/or CD36 blocking antibody (FA6-152) for 24h (n=4). Values are normalized to the number of viable cells per condition and reported as a fold change to control. Values are expressed as mean ± SEM. a, Mann-Whitney or unpaired t test depending on sample distribution, with or without Welch's correction depending on sample variance. b, Wilcoxon matched-pairs signed rank test. d, one sample t test. e-h, ordinary two-way ANOVA. j-aa, ordinary one-way ANOVA with Tukey's multiple comparisons test. *P<0.05, **P<0.01, ***P<0.001, ****P<0.0001.

Fig. S2. CD36 triggers OCIAML3 migration and analysis of blasts dissemination in vivo. a. GSEA gene signature of "GO_POSITIVE_REGULATION_OF_MONONUCLEAR_ CELL_MIGRATION" was performed in CD36 overexpressing patients from BEATAML, Verhaak and TCGA cohorts compared to the baseline CD36 expressers. **b-c.** Number of migrating cells in shCtrl or shCD36 OCIAML3 cells (**b**) and in siCtrl or siCD36 OCIAML3 cells (**c**) in the lower chamber of the transwell assay. Data are normalized to shCtrl/siCtrl for each experiment (n=8 and n=3). **d.** Number of migrating OCIAML3 cells treated or not with CD36 blocking antibodies (FA6-152 or JC63.1 as indicated) in the lower chamber of the transwell assay. Data are normalized to control (n=3). **e.** TSP1 mRNA expression in shCtrl or shTSP1 U937 cells. Data are normalized to shCtrl (n=3). **f.** TSP1 mRNA expression in shCtrl or shTSP1 OCIAML3 cells. Data are normalized to shCtrl (n=3). **g.** Number of migrating shCtrl or shTSP1 OCIAML3 cells in the lower chamber of the transwell assay. Data are normalized to control (n=3). **h.** Number of migrating shCtrl or shCD36 OCIAML3 cells in the lower chamber of the transwell assay, in the presence or absence of TSP1 blocking antibody (A6.1). Data are normalized to shCtrl (n=5). **i.** Number of migrating OCIAML3 cells treated or not with recombinant TSP1, in the presence or not of CD36-blocking antibody (FA6-152). Data are normalized to control (n=3). **j.** Acquisition of bioluminescent signals from organs harvested from mice injected with the indicated AML cell line stably expressing a luciferase reporter, at final time point. **k.** Quantification of bioluminescent signals in each organ (percentage compared to total bioluminescent signal). **l.** Quantification of human cells in the bone marrow (BM), spleen (SP), perigonadal adipose tissue (PGAT), and liver after intra-venous injection of U937 cells in NSG mice by RT-qPCR (n=2-3). hCD45 mRNA normalized to m36B4, data expressed as $2\Delta Ct$ (values multiplied by 1000). **m.** Flow cytometry analysis of human viable CD45+ AML blasts in the bone marrow (BM), spleen (SP), subcutaneous adipose tissue (SCAT), perigonadal adipose tissue (PGAT), liver, lung and blood 24 days after intra-venous injection of OCIAML3 (n=6). Values are expressed as mean ± SEM. **n.** OCIAML3 cells incubated with IGG or FA6-152 anti-CD36 antibody (1 µg/ml) for 30 minutes were injected intra-venously in NSG mice. Mice were treated with either control IgG or FA6-152 anti-CD36 antibody injected 3 times/week. At day 10 after injection, tumor burden was analyzed by flow cytometry in different organs including bone marrow (BM), perigonadal adipose tissue (PGAT), liver and lung. a, unpaired t test with or without Welch's correction depending on sample

variance. b-h, one sample or Wilcoxon t test depending on sample distribution. i, ordinary one-way ANOVA with Tukey's multiple comparisons test. n. Mann-Whitney tests. *P<0.05, **P<0.01, ***P<0.001, ****P<0.0001.

Fig. S3. Effect of AraC on monocytes markers expression and senescence in OCIAML3 cells, and PDX TUH07 single-cell RNAseq correlation plots. a. CD11b, CD14, CD15 and CD44 cell surface expression in viable OCIAML3 cells in control conditions or in the presence of 10µM AraC for 96h (n=4). **b**. FSC/SCC analysis on gated CD36low and CD36high cells from OCIAML3 treated or not with 10µM AraC for 4 days (n=3). **c.** C12FDG staining (MFI) in gated CD36low and CD36high OCIAML3 cells treated or not with 10µM AraC for 4 days. Data are normalized to control CD36low cells (n=3). **d.** Expression of senescence-associated genes in AraC-treated OCIAML3 cells expressed as a Log2 fold change in comparison to untreated cells. mRNA of the gene of interest was normalized to the human housekeeping gene, data expressed as 2ΔΔCt. Data are normalized to control (n=3). **e.** C12FDG staining on OCIAML3 cells treated or not with 10µM AraC and CD36 blocking antibody (FA6-152) for 4 days. Data are normalized to control (n=4). **f-g.** U937 cells were treated with 2µM AraC for 4 days and viable cells were FACS sorted and submitted to migration assay. C12FDG staining was then performed in migrating and non-migrating cells. **f.** Representative histogram of C12FDG staining in non-migrating and migrating AraC-treated cells. **g.** Quantification of C12FDG staining performed in **f.** Data are normalized to non-migrating AraC-treated cells (n=4). **h.** Correlation between expression levels of gene sets related to migration (WU_CELL_MIGRATION) and the CD36 gene signature. **i.** Correlation between expression levels of gene sets related to senescence (FRIDMAN_SENESCENCE_UP) and the CD36 gene signature. **j.** Correlation between expression levels of gene sets related to senescence (FRIDMAN_SENESCENCE_UP) and migration (WU_CELL_MIGRATION). Values are represented as mean ± SEM. a and b, Mann-Whitney or unpaired t test depending on sample distribution, with or without Welch's correction depending on sample variance. c and e, ordinary one-way ANOVA with Tukey's multiple comparisons test. d and g, one sample t test. *P<0.05, **P<0.01, **P<0.001, ****P<0.0001.

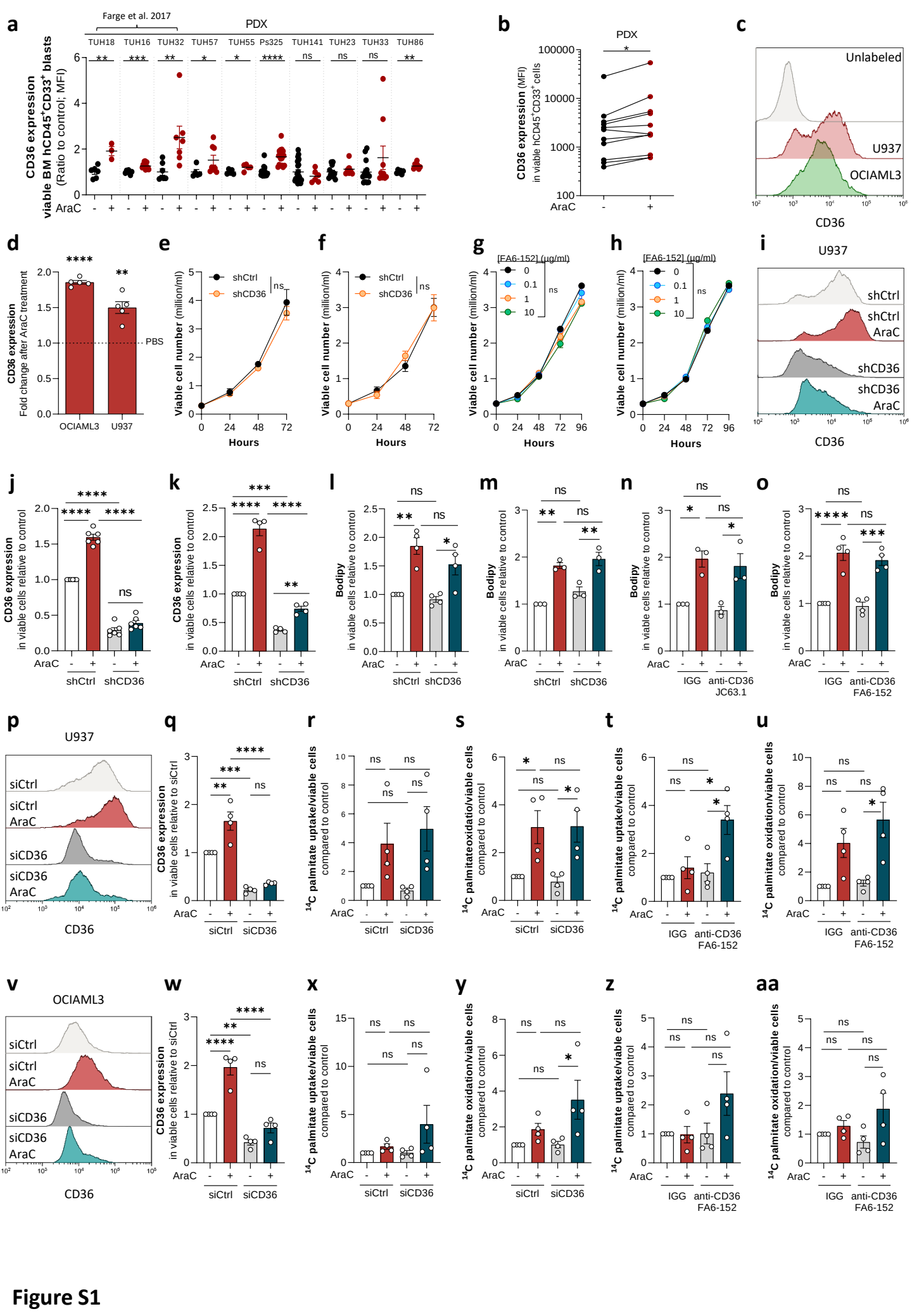
a
Farge et al. 2017
PDX
TUH18
TUH16
TUH32
TUH57
TUH55
Ps325
TUH141
TUH23
TUH33
TUH86
CD36 expression
viable BM hCD45+CD33+ blasts
(Ratio to control; MFI)
AraC
b
PDX
CD36 expression (MFI)
in viable hCD45+CD33+ cells
AraC
c
Unlabeled
U937
OCIAML3
CD36
d
CD36 expression
Fold change after AraC treatment
PBS
OCIAML3
U937
e
shCtrl
shCD36
Viable cell number (million/ml)
Hours
f
shCtrl
shCD36
Viable cell number (million/ml)
Hours
g
[FA6-152] (µg/ml)
0
0.1
1
10
Viable cell number (million/ml)
Hours
h
[FA6-152] (µg/ml)
0
0.1
1
10
Viable cell number (million/ml)
Hours
i
U937
shCtrl
shCtrl AraC
shCD36
shCD36 AraC
CD36
j
CD36 expression
in viable cells relative to control
AraC
shCtrl
shCD36
k
CD36 expression
in viable cells relative to control
AraC
shCtrl
shCD36
l
Bodipy
in viable cells relative to control
AraC
shCtrl
shCD36
m
Bodipy
in viable cells relative to control
AraC
shCtrl
shCD36
n
Bodipy
in viable cells relative to control
AraC
IGG
anti-CD36 JC63.1
o
Bodipy
in viable cells relative to control
AraC
IGG
anti-CD36 FA6-152
p
U937
siCtrl
siCtrl AraC
siCD36
siCD36 AraC
CD36
q
CD36 expression
in viable cells relative to siCtrl
AraC
siCtrl
siCD36
r
14C palmitate uptake/viable cells
compared to control
AraC
siCtrl
siCD36
s
14C palmitateoxidatio/viable cells
compared to control
AraC
siCtrl
siCD36
t
14C palmitate uptake/viable cells
compared to control
AraC
IGG
anti-CD36 FA6-152
u
14C palmitate oxidation/viable cells
compared to control
AraC
IGG
anti-CD36 FA6-152
v
OCIAML3
siCtrl
siCtrl AraC
siCD36
siCD36 AraC
CD36
w
CD36 expression
in viable cells relative to siCtrl
AraC
siCtrl
siCD36
x
14C palmitate uptake/viable cells
compared to control
AraC
siCtrl
siCD36
y
14C palmitate oxidation/viable cells
compared to control
AraC
siCtrl
siCD36
z
14C palmitate uptake/viable cells
compared to control
AraC
IGG
anti-CD36 FA6-152
aa
14C palmitate oxidation/viable cells
compared to control
AraC
IGG
anti-CD36 FA6-152

Figure S1

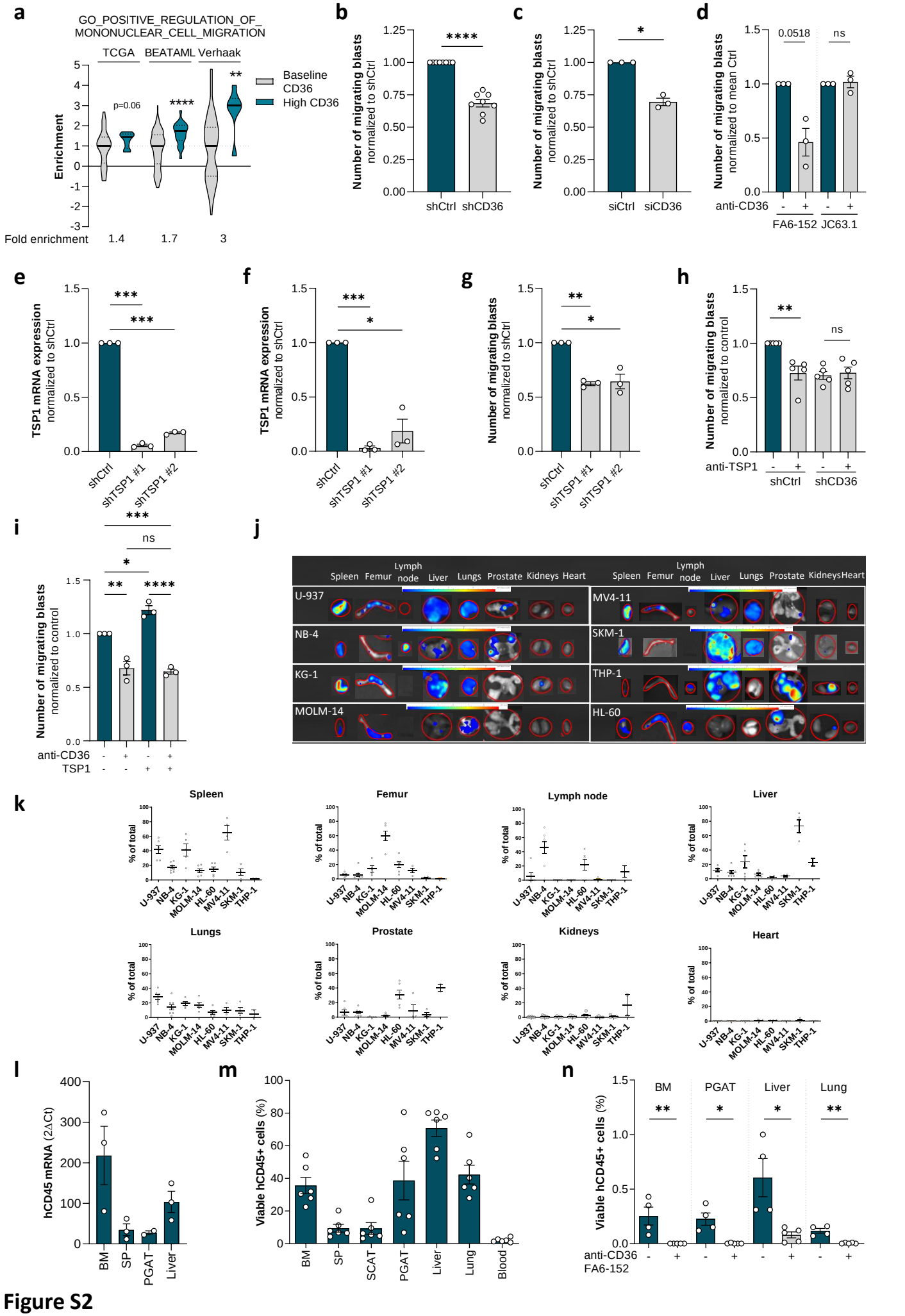
a
GO_POSITIVE_REGULATION_OF_MONONUCLEAR_CELL_MIGRATION
TCGA
BEATAML
Verhaak
Baseline
CD36
High CD36
Enrichment
p=0.06
****
**
Fold enrichment
1.4
1.7
3
b
Number of migrating blasts
normalized to shCtrl
****
shCtrl
shCD36
c
Number of migrating blasts
normalized to shCtrl
*
siCtrl
siCD36
d
Number of migrating blasts
normalized to mean Ctrl
0.0518
ns
anti-CD36
FA6-152
JC63.1
e
TSP1 mRNA expression
normalized to shCtrl
***
***
shCtrl
shTSP1 #1
shTSP1 #2
f
TSP1 mRNA expression
normalized to shCtrl
***
*
g
Number of migrating blasts
normalized to shCtrl
**
*
h
Number of migrating blasts
normalized to control
**
ns
anti-TSP1
shCtrl
shCD36
i
Number of migrating blasts
normalized to control
***
ns
*
**
****
anti-CD36
TSP1
j
Spleen
Femur
Lymph node
Liver
Lungs
Prostate
Kidneys
Heart
U-937
NB-4
KG-1
MOLM-14
MV4-11
SKM-1
THP-1
HL-60
k
Spleen
Femur
Lymph node
Liver
Lungs
Prostate
Kidneys
Heart
% of total
l
hCD45 mRNA (2ΔCt)
BM
SP
PGAT
Liver
m
Viable hCD45+ cells (%)
BM
SP
SCAT
PGAT
Liver
Lung
Blood
n
Viable hCD45+ cells (%)
BM
PGAT
Liver
Lung
**
*
*
**
anti-CD36
FA6-152

Figure S2

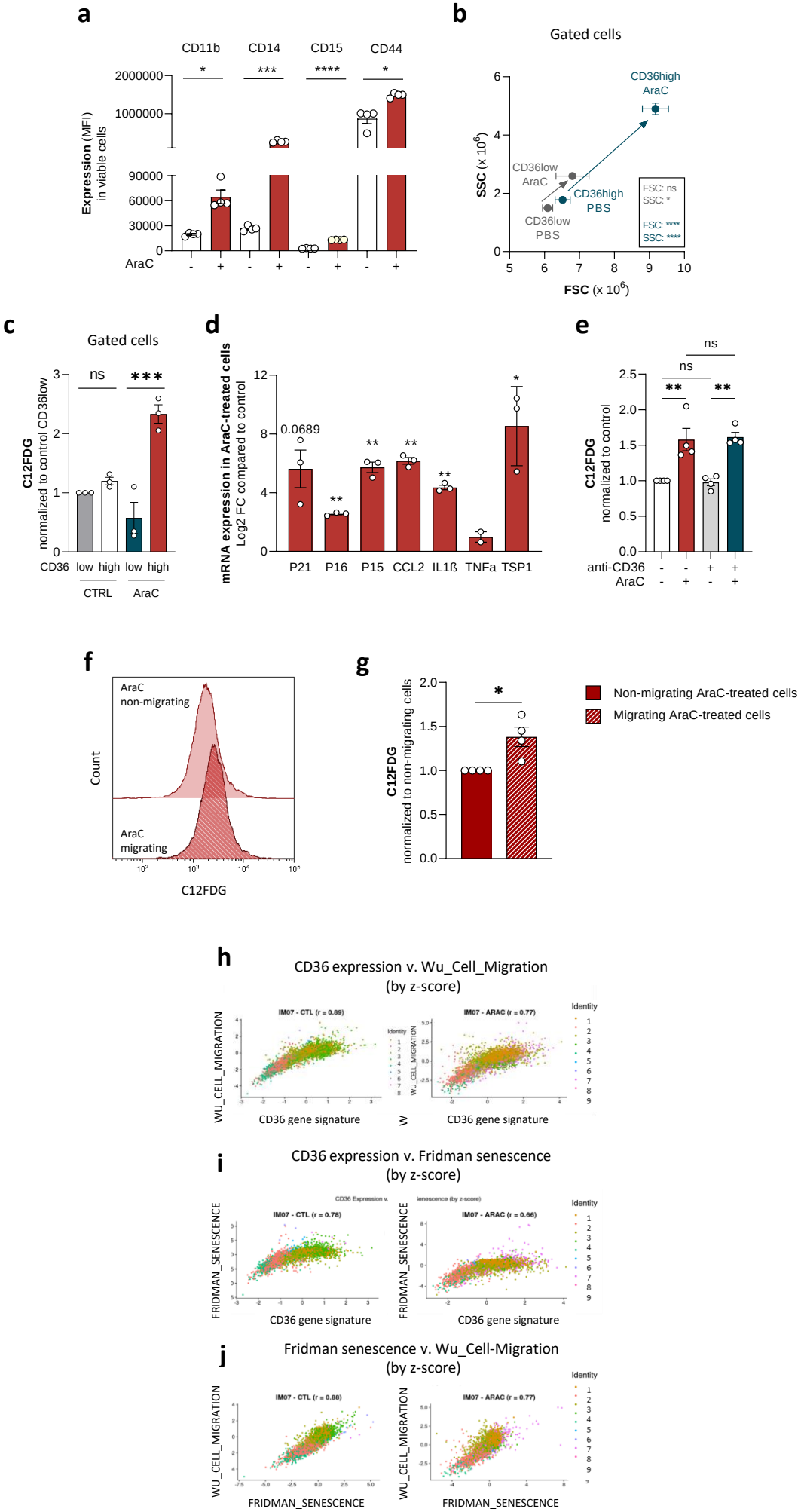
a
CD11b
CD14
CD15
CD44
Expression (MFI) in viable cells
AraC
b
Gated cells
CD36high AraC
CD36low AraC
CD36high PBS
CD36low PBS
SSC (x 10^6)
FSC (x 10^6)
FSC: ns
SSC: *
FSC: ****
SSC: ****
c
Gated cells
C12FDG normalized to control CD36low
CD36 low high low high
CTRL
AraC
d
mRNA expression in AraC-treated cells Log2 FC compared to control
0.0689
P21 P16 P15 CCL2 IL1ß TNFa TSP1
e
C12FDG normalized to control
anti-CD36
AraC
f
AraC non-migrating
AraC migrating
Count
C12FDG
g
C12FDG normalized to non-migrating cells
Non-migrating AraC-treated cells
Migrating AraC-treated cells
h
CD36 expression v. Wu_Cell_Migration (by z-score)
IM07 - CTL (r = 0.89)
IM07 - ARAC (r = 0.77)
WU_CELL_MIGRATION
CD36 gene signature
Identity
i
CD36 expression v. Fridman senescence (by z-score)
IM07 - CTL (r = 0.78)
IM07 - ARAC (r = 0.66)
FRIDMAN_SENESCENCE
CD36 gene signature
j
Fridman senescence v. Wu_Cell-Migration (by z-score)
IM07 - CTL (r = 0.88)
IM07 - ARAC (r = 0.77)
WU_CELL_MIGRATION
FRIDMAN_SENESCENCE

Figure S3